Strategies and Applications for Visible Light Mediated Photoredox Transformations in Organic Chemistry

Sven Bourgeois

A thesis submitted in partial fulfillment of the requirements for the

Master of Science degree in Chemistry

Department of Chemistry and Biomolecular Sciences

Faculty of Science

University of Ottawa

Abstract

The field of photoredox catalysis has emerged as a prominent approach to synthetic chemistry over the past decade, offering powerful strategies in the activation of small molecules. Many of these systems have been proven to perform efficiently and with high selectivity under milder conditions compared to thermally driven reactions. These systems are instead powered by cheap and widely available light sources which excite catalysts capable of converting visible light into useful chemical energy. In general, this process is mediated by the engagement of organic substrates with the excited catalyst via single electron transfer events to produce reactive intermediates. However, despite these advantages there are currently only a limited number of photoredox catalysts available, almost all of which are based on iridium and ruthenium complexes. These precious earth-scarce metal catalysts are extremely expensive, toxic and difficult to manufacture, in addition to usually offering nothing with regards to recyclability. The field is also lacking a full understanding of the complete underlying mechanistic pathways responsible for these transformations.

Herein, examples of a cheap and widely available nickel complex as an all-in-one photocatalyst and cross-coupling agent will be introduced in the direct C-H coupling of ethers to boronic acids. To the best of our knowledge, this is the first example of this type of multifunctionality for photochemistry and cross-coupling in a nickel catalyzed system. Additionally, the translation of the important Heck reaction into a heterogeneous, photochemically driven system will be demonstrated. The inorganic

composite semiconductor Au@TiO_2 can be used to harvest visible light to facilitate the coupling of olefins at an unprecedented combination of low temperature and lower cost, while providing exceptionally high turnover rates and recycling capabilities. Finally, this work will illustrate the use of aluminum oxide as a heterogeneous catalyst for the coupling of aryl chlorides to amines. Although not photochemically catalyzed, this particular work illustrates the ability of a cheap and abundant material to promote reactivity of ubiquitous aryl chlorides in a fully heterogeneous matter.

Overall, the contents of this thesis report the development and implementation of lower cost and bench-stable catalytic systems capable of contending with their predecessors while simultaneously offering simple, facile separation of catalysts and reagents.

Acknowledgements

Acknowledgments

I am very grateful to have been given the opportunity to conduct my graduate studies in the Scaiano group. It has truly been an enriching experience to learn and grow alongside such a large group of passionate researchers from across the globe. The expertise and equipment available both in the group and the department as a whole are unparalleled in quality. Over the past few years, meeting and collaborating with a fantastic group of people, combined with a great workspace, has helped shape me into the person I am today and achieve my goals.

While there are many people I would like to thank and give due credit, I must first and foremost thank Tito, who has been an outstanding supervisor and mentor over the years. Beginning with my Honours project under his supervision, I was inspired to research more complex ideas and learn more advanced techniques as I continued into graduate work. I was always given the freedom to explore my own ideas and this fostered creativity has further allowed me to develop the knowledge and critical thinking skills I can take with me on my future endeavours.

Further, I'd like to thank Spencer Pitre for his patience in helping out a new graduate student and passing along much of his knowledge of photoredox chemistry. I would like to thank Betty Yakimenko for making administrative tasks a breeze and run so smoothly. Thank you to Michel Grenier for technical support in the setup and troubleshooting of our instrumentation. I want to thank Anabel Lanterna for all her

support over the years, providing valuable advice when discussing projects and editorial feedback. A huge thank you to all my fellow colleagues and graduate students both past and present that I have had the pleasure to work with. Their support on the day-to-day and in group meetings has been both motivational and tremendously helpful at gaining new insights on projects and seeing my research from a different perspective.

Finally, I must thank my friends and family for their support throughout this journey. Their encouragement along the way is deeply appreciated even if they have not always understood the path I chose to take.

Thank you all so much!

Contribution Statement

Contribution Statement

All of the projects presented in this thesis were completed under the guidance and supervision of Dr. Juan (Tito) Scaiano. Working in the Scaiano group over the course of my graduate studies has given me the opportunity to work with a diverse group of graduate students in a multidisciplinary environment, allowing me to collaborate with my colleagues and combine our expertise on various projects. On that account, while the majority of the work presented in this thesis came about as a result of independent research, I wanted to highlight not only the contributions made directly by myself but also those of my collaborators in the following section.

The work presented on light-mediated C-H arylations involving a nickel catalyst was one of the earlier projects I worked on upon joining the Scaiano group. The original idea to utilize a boronic acid as a coupling partner in a photoredox/nickel dual catalytic system was conceived by Spencer Pitre, a former Ph.D. student in the Scaiano group. With a strong background in photoredox catalysis, he also provided valuable insights and guidance at the beginning of my graduate work. The synthesis of titanium dioxide supported palladium nanoparticles, which was used as a test catalyst to see if the system could be totally heterogenized, was carried out by Ayda Elhage.

The use of alumina as a catalyst in the coupling of aryl chlorides with amines was an independent project started by myself to explore the catalytic ability of naked alumina after an oversight was evidently made in a previously published report by an external research group. The Murugesu lab generously offered use of their microwave reactor and corresponding equipment.

The work on heterogeneous, visible light mediated Heck reactions was initiated by myself but originally utilized copper nanoparticles supported on titanium dioxide. The use of titanium dioxide supported gold nanoparticles as a model catalyst in addition to the employment of benzyl halides instead of potassium trifluoroborate salts were suggestions made by Anabel Lanterna, a research associate in the Scaiano group. Anabel was also involved in many of the discussions throughout all these projects to provide her own expertise in nanomaterials.

Table of Contents

List of Figures

List of Schemes

List of Tables

List of Abbreviations

*	excited state
[ ]	concentration
‡	transition state
^{1}H	hydrogen nucleus (proton)
4-NBB	4-nitrobenzyl bromide
acac	acetylacetonate
$Au@TiO_2$	gold supported on titanium dioxide
BDE	bond dissociation energy
BHT	butylated hydroxytoluene
CB	conduction band
C-C	carbon-carbon
C-H	carbon-hydrogen
Chloroform-d	deuterated chloroform
d	doublet
DCM	dichloromethane
DIPEA	N,N-Diisopropylethylamine
dtbbpy	4,4’-di-tert-butyl-2,2’-dipyridyl
DTBP	di-tert-butyl peroxide
E	energy
e^{-}	electron

EA	electron affinity
E_{bg}	band gap energy
EDG	electron donating group
eq.	equivalents
EWG	electron withdrawing group
GC-MS	gas chromatography-mass spectrometry
h	Planck's constant
h^+	hole
HOMO	highest occupied molecular orbital
Hz	hertz
hν	light
IP	ionization potential
J	coupling constant
J	Joule
LED	light emitting diode
LEDi	light emitting diode illuminator
LUMO	lowest unoccupied molecular orbital
m	multiplet
MLCT	metal-to-ligand charge-transfer
ND	not detected
NIR	near infrared
nm	nanometer

NMR	nuclear magnetic resonance
NP	nanoparticle
Nu	nucleophile
PC	photocatalyst
PPh_3	triphenylphosphine
ppm	parts per million
ppy	2-phenylpyridine
PTLC	preparatory thin layer chromatography
q	quartet
R	rectus
redox	reduction-oxidation
RPM	rotations per minute
RT	room temperature
S	sinister
SET	single electron transfer
S_x	singlet state
t	triplet
THF	tetrahydrofuran
T_x	triplet state
UV	ultraviolet light
UVA	ultraviolet A
UVB	ultraviolet B

VB	valence band
VIS	visible light
X	halide
δ	chemical shift
λ	wavelength
ν	frequency

1. Introduction

1.1. Opening Remarks

The work presented in this thesis is focused on the application of photoredox processes toward organic transformations. The objective is to demonstrate that light can be used to power reactions that otherwise would require harsh conditions or expensive materials; the latter of which has received little attention in the field's development. This work also examines the adaptation of heterogeneous materials as a more sustainable alternative to traditional homogeneous catalysts. The first chapter of this work outlines the fundamentals of photochemistry, photoredox catalysis and heterogeneous materials to better understand the operations at play. Chapter 2 summarizes an attempt to apply photoredox catalysis to a published methodology and ultimately demonstrate how a lack of control experiments can lead to misleading literature. Chapter 3 investigates the use of heterogeneous TiO_2 as an alternative photocatalyst to the commonly used homogeneous iridium and ruthenium complexes, as well as deploying a substitute for palladium catalysts to perform cross-coupling under atypically mild conditions. Lastly, chapter 4 focuses on the use of TiO_2 supported gold nanoparticles as a heterogeneous method to catalyze Mizoroki-Heck type cross-coupling reactions utilizing vinyl arenes and visible light. The following few sections will facilitate a better understanding of the results presented within the body of this work.

1.2. Introduction to Photochemistry

Photochemistry is concerned with the chemical changes that occur following the interactions of light with matter. For a photochemical process to begin, a molecule must first be physically capable of absorbing photons (hv) at a given frequency. When the energy absorbed is high enough, the molecule can excite an electron from a ground-state electronic level to another level of higher energy. Figure 1.1 depicts a simplified Jablonski diagram which shows many of the potential processes a molecule can experience after the absorption of a photon. Electrons are promoted from the highest unoccupied molecular orbital (HOMO) of a molecule to a singlet state, where the excited state electron pair retains its antiparallel spin configuration. The electron is typically directly excited into a higher vibrational level of the first or second excited singlet state (S_1 and S_2, respectively) during this process. However, internal conversion almost always occurs, demoting the electron to the lowest vibrational level of S_1 before any other events[1]. This non-radiative decay phenomenon releases the energy in the form of heat and is known as Kasha's rule[2]. From the singlet state, excited electrons may in some cases undergo intersystem crossing which flips the spin of one electron to create an excited triplet state that has a spin parallel configuration. The inversion of spin on an electron is quantum mechanically forbidden and thus becomes a slow event. Although some molecules like benzophenone perform this function very efficiently, the low probability of this event generally leads to extended lifetimes from the triplet state as relaxation to the ground state cannot occur without a spin flip; doing so would violate the Pauli exclusion principle[3].

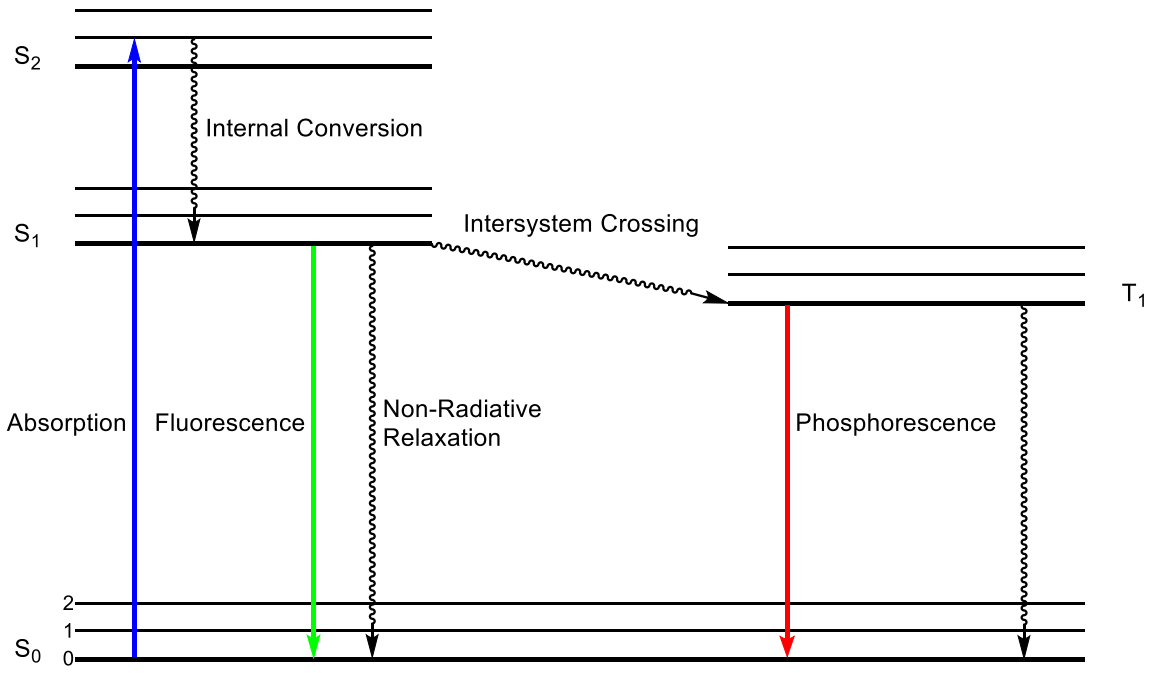

Figure 1.1. Jablonski diagram representing energy relation on the vertical axis and spin configuration on the horizontal axis.

The excitation of a molecule also has an affect on its redox properties. Typical redox reagents are quite reactive and are most often used in stoichiometric amounts, as oxidation or reduction occurs from their ground states. Even though these ground state oxidants and reductants can perform the same chemical transformations as their excited state counterparts, their reactivity inherently makes them more difficult to work with. A great advantage of photoredox is its ability to overcome these limitations in organic transformations by generating redox states through photoexcitation, where the redox material may cycle between a more reactive excited state and more inert ground state. These agents are even capable of being deployed catalytically, as will be explored in section 1.4.

In recent photoredox literature, there have been many cases where a photocatalyst is presented to be a better electron donor or acceptor from its excited state, with little explanation as to why. The reality is that any closed shell, diamagnetic molecule will have this effect from its singlet or triplet excited state. When excitation occurs, there is an increase to the electron affinity (EA) and a decrease to the ionization potential (IP) of the excited molecule, compared to its corresponding ground state (Figure 1.2). Thermodynamically speaking, the addition of an electron to the half-filled HOMO yields a larger release of energy than if the addition occurred to the LUMO of the ground state molecule. Conversely, the removal of an electron from the excited state requires less energy than would be necessary to remove one from the HOMO of the ground state, thus creating a more oxidizing and reducing species after excitation.

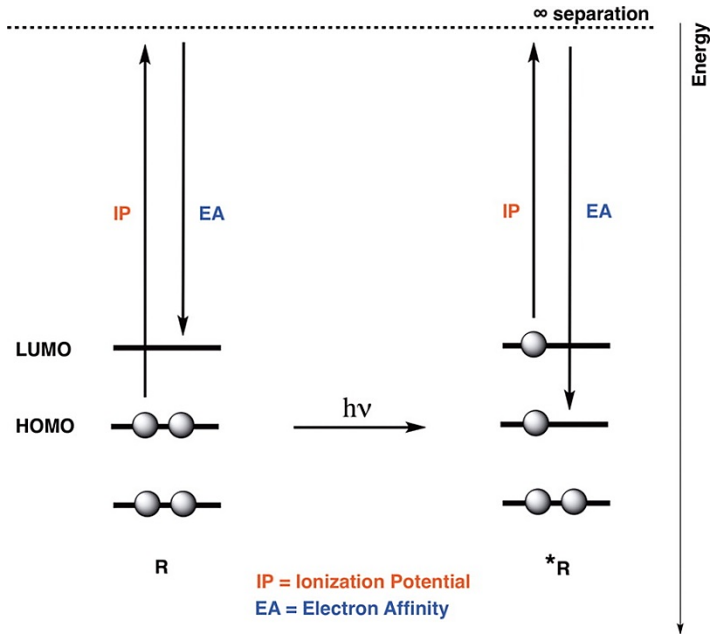

Figure 1.2. Orbital energy level diagram for the redox processes of ground state and excited state closed shell species. Adapted with permission from Turro *et al.*[4] Copyright 2010 University Science Publishers.

The characteristics discussed here are also universal and not limited to just specific sets of molecules, so long as they are diamagnetic and have a closed shell. To illustrate this, one could even excite a helium atom and the resulting excited state would be more reducing than lithium in the ground state (Figure 1.3). This example is of course unreasonable for practical use as the energy difference between the HOMO and LUMO for helium is 2,000 kJ/mol and would require an excitation wavelength of at least 60 nm but the principle is all the same. This does however illustrate a limitation of photoredox species, that their excitation energies must fall within reasonable limits both for their practical implementation with a light source and to ensure that there is no competitive absorption by other components including the reaction container.

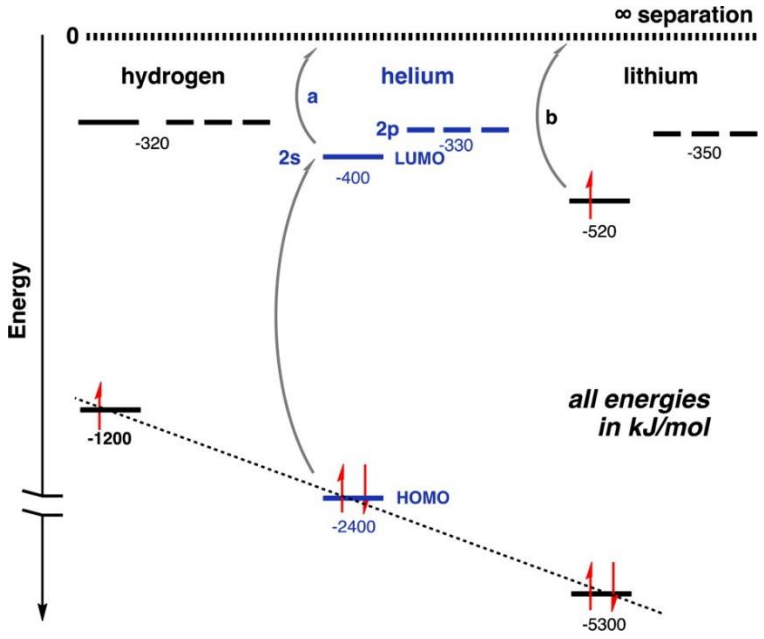

Figure 1.3. Orbital energy level comparison for hydrogen, helium and lithium. The ionization potential of excited helium (a) is less than that of ground state lithium (b), making it the more reducing species. Adapted with permission from Pitre *et al.*[5] Copyright 2016 American Chemical Society.

1.3. Introduction to Photoredox Catalysis

Traditional cross-coupling catalysis has been dominated by homogeneous noble metal materials and although modern catalysts are able to perform difficult transformations with high selectivity and efficiency, they suffer from high costs, difficult syntheses and are often sensitive to air and moisture.[6–9] This inherently reduces their availability and ease of use, both on the bench and on the industrial scale. Although there has been a push to replace these metals with more widely available non-precious ones (base metals), these catalysts often perform significantly worse than their noble counterparts in all other contexts, requiring higher loadings and harsher conditions for their operation as well as having shorter lifespans and overall reduced activity.[10–16]

In a general sense, the basis for transition metal catalytic activity is in the facile formation, rearrangement and subsequent elimination of organometallic bonds from either a single substrate (homocoupling) or multiple substrates (heterocoupling). Scheme 1.1 depicts a generic Suzuki-Miyaura coupling, perhaps the most well studied example of transition metal catalyzed cross-coupling reactions. In this system, an aryl halide can be both directly activated by and added to the metal species through an oxidative addition step. The oxidized metal complex becomes too electron deficient to afford another oxidative addition and instead may selectively undergo a redox neutral transmetalation with a boronic acid. This engagement brings both moieties into proximity to assist C-C bond formation while reducing the metal, closing the catalytic cycle. This ultimately enables the use of two different coupling partners while

suppressing homocoupling between two molecules of the same reactant. However, like most other metal-catalyzed systems, Suzuki coupling relies on the use of activated substrates like halogenated arenes to perform key insertion steps onto the catalyst. This makes reagents more expensive and increases the difficulty of late stage syntheses where these activating groups may not always be applicable to more complex scaffolds.

Scheme 1.1. A generalized Suzuki-Miyaura coupling between an aryl halide and a boronic acid.

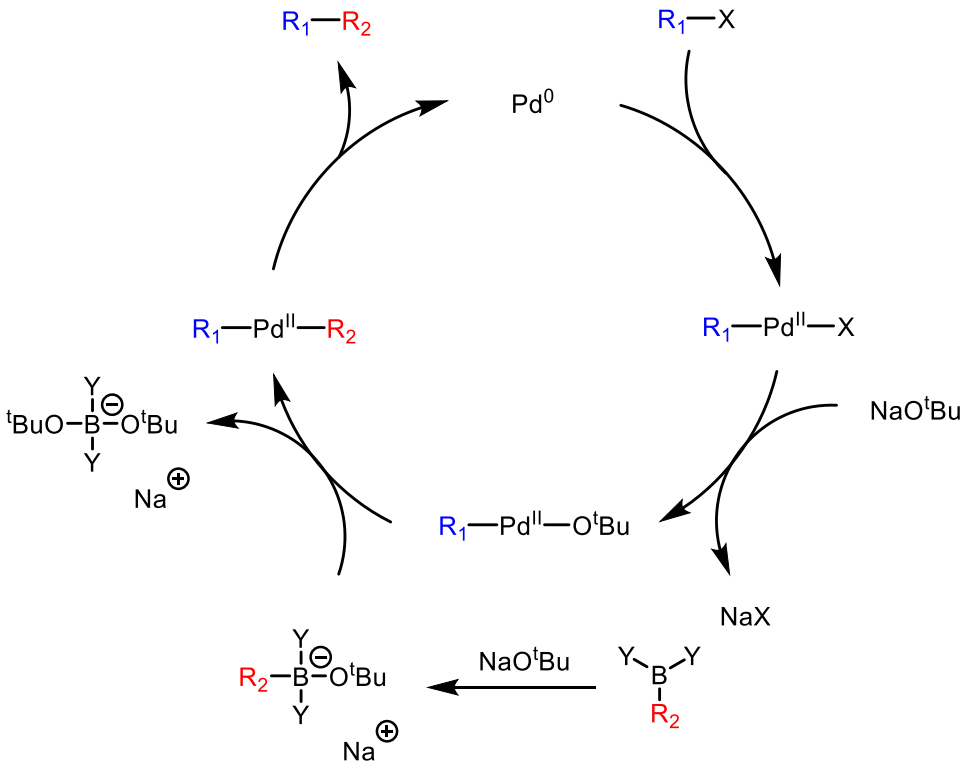

Photoredox offers an alternative method in two ways; (1) the catalytic cycle is light-activated and (2) the catalyst is not directly involved as an intermediate in the coupling process. Typically, light from the visible spectrum is used to excite a photosensitizer into an excited state, which acts as a reducing or oxidizing agent for the chosen substrate. The substrate undergoes a one electron addition or removal to

generate an open shell reactive intermediate that can independently engage with other species to perform many different organic transformations. The photosensitizer is replenished by a late stage intermediate to turn over its cycle and repeat the process (Scheme 1.2).

Scheme 1.2. A generalized photoredox catalytic cycle with oxidative and reductive pathways, where PC is the photocatalyst.

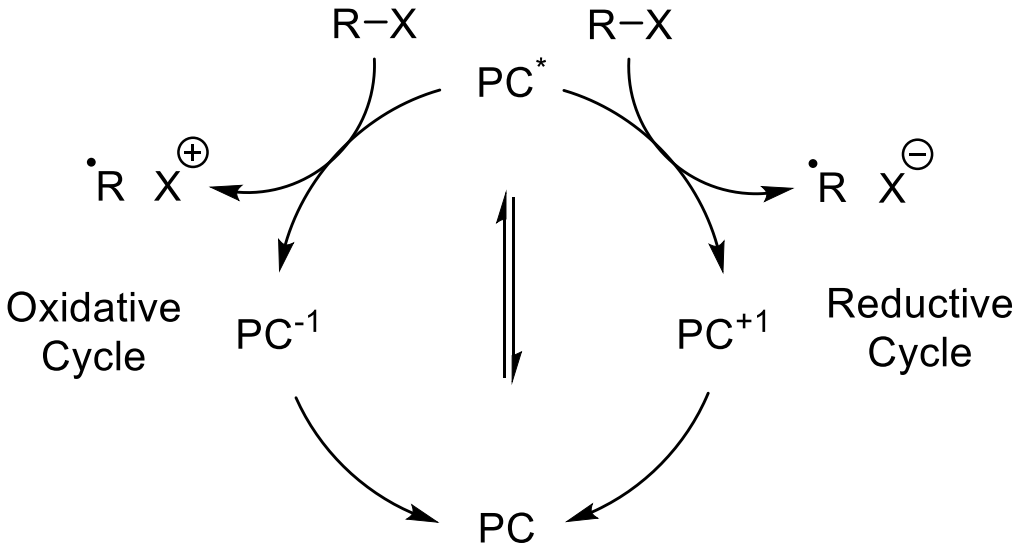

Although photoredox catalysts may take many different forms, the most popular are organometallic complexes of Ru and Ir.[17] These complexes offer robust character, so they degrade little even with prolonged irradiation times and may be employed in very small amounts, owing to their high efficiency in absorbing light to create excited state complexes through metal-to-ligand charge-transfer (MLCT). Additionally, these catalysts display long excited state lifetimes, increasing the likelihood of a redox event with another molecule before relaxation occurs. By selecting which metal centers are used and what ligands are present, the redox properties of each catalyst can be fine-tuned to specific redox potentials that will selectively engage targeted substrates.

A good example of the implementation of photoredox catalysis is demonstrated through the work of Nicewicz on the nucleophilic substitution of arenes.[18] In older methodologies, these substitutions would commonly be performed at high temperatures and require strong electron withdrawing groups (EWG) on the aromatic system both as activators and as leaving groups.[19] This has been proposed to allow for the formation and stabilisation of the Meisenheimer or sigma complex which acts as a highly energetic transition state as it contains one quaternary carbon within the ring system (Scheme 1.3).[20] As most of the EWGs used are fluoride, chloride or nitro groups, their removal also generates a stochiometric amount of those species in solution, often abstracting protons from the nucleophile. Even the alternative electrophilic aromatic substitution reaction, which does not require activating groups, still must use a Lewis acid catalyst like aluminum trichloride to proceed.[21,22] This catalyst must be present in large, usually super-stoichiometric amounts to work properly and results in a toxic sludge that must be dealt with after use. Problems of this type also show up in more modern catalytic approaches like Buchwald-Hartwig amination where there is greater tolerance for activating groups but at the cost of using copper or palladium catalysts that still require an EWG leaving group.[23–25]

Scheme 1.3. Mechanistic pathway for nucleophilic substitutions showing the proposed sigma complex transition state.

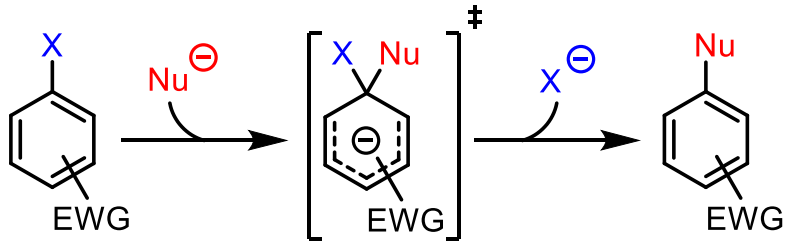

When this substitution reaction is carried out using an acridinium photoredox catalyst in Nicewicz' example, several benefits are applied that negate the shortcomings of the previous examples. The first is the employment of an inexpensive and less toxic photocatalyst at a modest 5 mol% loading, that is operated using a common aquarium LED lamp. The substrates also do not need strongly withdrawing activating groups or leaving groups. Upon excitation, the photocatalyst selectively oxidizes the aromatic ring to a radical cation, unlike any pathway of the other examples. This newly formed intermediate is a great electrophile and will accept a wide range of nucleophilic partners including various amines and alcohol functional groups before a reductive quench replenishes the photocatalyst and the aromaticity of the ring. Typically, a methoxy handle was used as an all-in-one directing group and leaving group which only generates methanol as a by-product. By using this method, far less constraints are placed onto what type of substrates can be used in the system, foregoing the production of harmful by-products in the process and overall reducing the cost of production. Interestingly, this catalyst could be used to also selectively depolymerize a model lignin substrate with guaiacol and veratrole motifs during the functionalization process in a redox neutral fashion. This valorises what is otherwise considered a waste product and has few commercial chemical uses.[26–28]

1.4. Semiconductor Photocatalysts

As previously discussed, photoredox catalysis offers many advantages over traditional cross-coupling reactions in part because of its ability to offer milder conditions for substrate activation. The iridium and ruthenium catalysts most widely used for photoredox reactions are still however limited by some of the same drawbacks as all the other homogeneous catalysts. Whenever a catalyst is added to the same phase as the reaction mixture, it must be separated out after the reaction is complete. This separation step usually involves chromatographic techniques that, when brought to large scale, consume enormous amounts of organic solvent. Particularly in the pharmaceutical industry, where regulations on impurities within a product are very strict, solvent may not be reusable and more may be required to achieve proper separation. The solvent used for workup and purification now becomes the biggest waste product of the overall production system and the cost of its removal a significant expense for the user, likely exceeding the cost of the raw material several times over.

The use of heterogeneous catalysts like zeolites, metallic powders and meshes has already been well implemented for use in the manufacture of many bulk chemicals that have relatively low molecular weights or few functionalities.[29] Their usage in industry has allowed for the facile isolation of the catalyst, rendering it mostly stationary with respect to the overall chemical process. Rather than moving all the components of the reaction through to workup, the insoluble and non-volatile catalyst can remain in the primary reaction vessel while products are removed.

A heterogeneous material with the right optical and catalytic properties could therefore be a suitable replacement to curb the major disadvantages of the typical iridium and ruthenium complexes employed. Fujishima and Honda demonstrated that TiO_2, a heterogeneous semiconductor, could be used for the photoelectrochemical splitting of water nearly 50 years ago[30]. This achievement has since sparked huge effort for the development of semiconductor-based catalysis and new uses for TiO_2, it also shows that a heterogeneous material has the potential to be used as a photoredox agent.

A semiconductor differs from a molecular photoredox agent in a few ways, but a parallel can still be drawn between the two in functionality (Figure 1.4). In a molecular species the excitation occurs between the HOMO and the LUMO with the HOMO being the site of the valence electrons. As more molecules are added to a lattice, the overlap of orbitals creates a "layer" of valence electrons and orbitals called the valence band (VB) which can encompass a range of energies as the HOMO no longer exists as a discreet entity. The valence band effectively represents the highest range of electronic population within a bulk material without any excitation. Similarly, the LUMO orbitals also overlap into a layer of electronic vacancies called the conduction band (CB). The band gap is the energetic barrier that exists between these two bulk states and determines how insulating (larger band gap) or conductive (smaller band gap) a material is. It should be noted that a metal or any other good conductor does not really have a band gap as conduction occurs from partially filled bands that take on the characteristics of both the valence and conduction bands. An insulator on the other

hand is the outcome of a sufficiently large band gap that any conduction would be very minor, owing to the material's high resistivity to it. A true semiconductor is any species that falls between these two extremes.

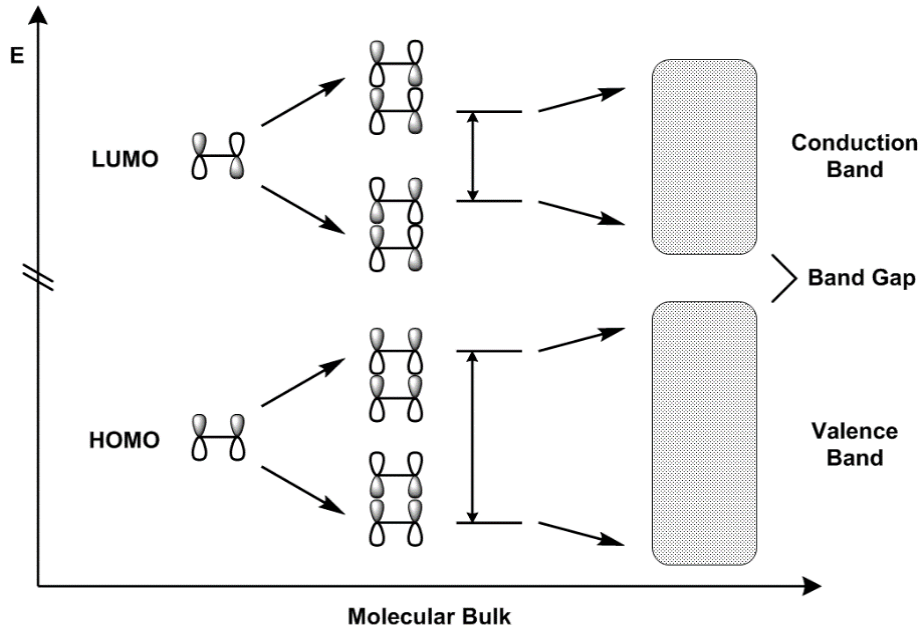

Figure 1.4. Energy level diagram comparison of a molecular species (left) and a bulk molecule semiconductor (right).

When electrons are excited into the conduction band, an electropositive deficit is also left behind in the valence band, called a hole (h^+). Together, this pair of separated charge carriers is known as an exciton and is analogous to the previously seen molecular excited state; it is both more oxidizing and reducing than it was in the ground state.

A limitation of semiconductors is how much energy is required for the excitation and what energy source is used. Light can be used as a direct way of overcoming the band gap energy, provided the energy of the incoming photon is at least equal in energy and the semiconductor can absorb it. However, different materials will have different

charge carrier kinetics and absorption alone will not determine if a semiconductor is a good candidate for a photoredox role. After the excitation event, recombination of the electron and hole may occur too rapidly for them to diffuse to the material surface where they may perform useful chemistry. Some strategies exist to combat these processes but usually involve doping in one form or another. By adding another element into the molecular framework of a semiconductor, one can alter the overall electronic structure as seen in figure 1.5. In a general sense, adding a more electron rich element will negatively dope (n-dope) the material and adding a more electron poor element will positively dope (p-dope) the material, in turn raising the valence band or lowering the conduction band, respectively.

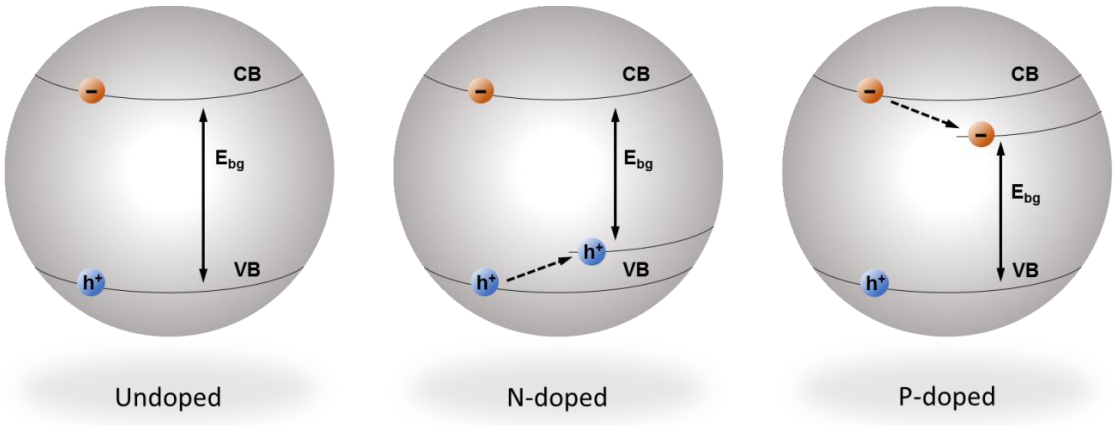

Figure 1.5. Effect of elemental doping on a semiconductor's band gap.

This doping process may shorten the band gap to accept longer wavelengths of light and require less energy but inherently results in a change to the redox properties of the material which may not be desirable. To avoid this situation, one may use an alternative method of doping semiconductors that involves decorating only the surface

with another material. The catalyst used in chapter 4 will use gold nanoparticles doped onto the surface of TiO_2 to mitigate some of its shortcomings and offer powerful advantages. The following section will use this material as an example to demonstrate this concept.

TiO_2 is perhaps one of the most well-known metal oxide semiconductors, it has gained popularity from its low cost, availability, ease of manufacture, recyclability and non-toxicity to name only a handful. Its main disadvantage is its bandgap of 3.2 eV, requiring light of approximately 365 nm to promote electrons into the conduction band. Gold nanoparticles on the other hand absorb light broadly in the visible region, the actual range will vary with particle size, but peak absorption commonly occurs at around 550 nm for the particles doped onto TiO_2. Only a small amount of metal is needed to achieve this effect, as little as 1% and in addition to the redshift in absorbance of the composite material, electrons populating the conduction band of the gold nanoparticles after plasmon activation are enabled to migrate into the conduction band of TiO_2 (Figure 1.6).[31–33]

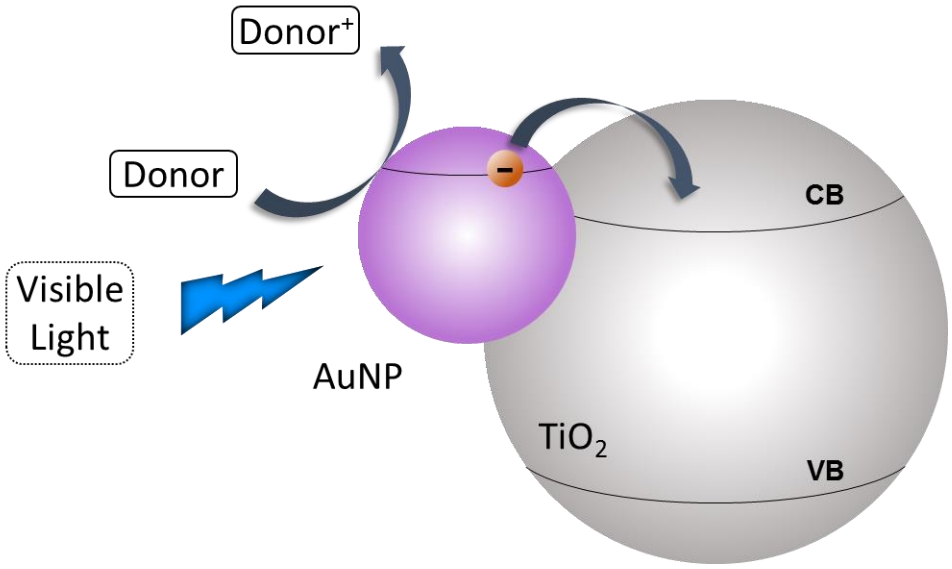

Figure 1.6. Diagram showing the proposed selective absorption of visible light by gold nanoparticles and subsequent transfer to TiO_2 CB before recombination.

The TiO_2 in this case is not simply an inert support but acts as a sort of trap for the electron, preventing rapid recombination of the electron-hole pair and extending its lifetime. Electrons injected into the conduction band of TiO_2 can be picked up by a suitable substrate in a reduction reaction, concurrently causing an electronic depletion within the gold nanoparticle and the creation of a hole. The electrons in Au@TiO_2 can be restored in a subsequent oxidative quench if a suitable electron donor is present. The hole that is generated after gold nanoparticle excitation also benefits from an extended lifetime even though it does not migrate into the support, due to the lack of electron population to recombine with. The catalyst can therefore function as both an oxidizer and reducing agent simultaneously, utilizing either the electron or the hole.

1.5. References

(1) Kasha, M.; McGlynn, S. P. *Annu. Rev. Phys. Chem.* **1956**, *7* (1), 403–424.

(2) Kasha, M. *Discuss. Faraday Soc.* **1950**, *9* (0), 14–19.

(3) Kasha, M.; Lewis, G. N. *J. Am. Chem. Soc.* **1944**, *66* (6), 2100–2116.

(4) Turro, N. J.; Ramamurthy, V.; Scaiano, J. C. *Modern Molecular Photochemistry of Organic Molecules*; University Science Publishers: New York, 2010.

(5) Pitre, S. P.; McTiernan, C. D.; Scaiano, J. C. *Acc. Chem. Res.* **2016**, *49* (6), 1320–1330.

(6) Biffis, A.; Centomo, P.; Del Zotto, A.; Zecca, M. *Chem. Rev.* **2018**, *118* (4), 2249–2295.

(7) Roy, D.; Uozumi, Y. *Adv. Synth. Catal.* **2018**, *360* (4), 602–625.

(8) Cordovilla, C.; Bartolomé, C.; Martínez-Ilarduya, J. M.; Espinet, P. *ACS Catal.* **2015**, *5* (5), 3040–3053.

(9) Medlock, J.; Bonrath, W. *Applications of Transition Metal Catalysis in Drug Discovery and Development: An Industrial Perspective*; 2013; Vol. 52.

(10) Lu, Z.; Wilsily, A.; Fu, G. C. *J. Am. Chem. Soc.* **2011**, *133* (21), 8154–8157.

(11) Gurung, S. K.; Thapa, S.; Kafle, A.; Dickie, D. A.; Giri, R. *Org. Lett.* **2014**, *16* (4), 1264–1267.

(12) Fan, S.; Chen, Z.; Zhang, X. *Org. Lett.* **2012**, *14* (18), 4950–4953.

(13) Wang, T. H.; Ambre, R.; Wang, Q.; Lee, W. C.; Wang, P. C.; Liu, Y.; Zhao, L.; Ong, T. G. *ACS Catal.* **2018**, *8* (12), 11368–11376.

(14) Filonenko, G. A.; Van Putten, R.; Hensen, E. J. M.; Pidko, E. A. *Chem. Soc. Rev.* **2018**, *47* (4), 1459–1483.

(15) Kurahashi, T.; Matsubara, S. *Acc. Chem. Res.* **2015**, *48* (6), 1703–1716.

(16) Fürstner, A. *ACS Cent. Sci.* **2016**, *2* (11), 778–789.

(17) Prier, C. K.; Rankic, D. A.; MacMillan, D. W. C. *Chem. Rev.* **2013**, *113* (7), 5322–5363.

(18) Tay, N. E. S.; Nicewicz, D. A. *J. Am. Chem. Soc.* **2017**, *139* (45), 16100–16104.

(19) Rajpara, V.; Banerjee, S.; Sereda, G. *Synthesis (Stuttg).* **2010**, *2010* (16), 2835–2840.

(20) Chéron, N.; El Kaïm, L.; Grimaud, L.; Fleurat-Lessard, P. *Chem. - A Eur. J.* **2011**, *17* (52), 14929–14934.

(21) Bensari, A.; Zaveri, N. T. *Synthesis (Stuttg).* **2003**, *2003* (2), 0267–0271.

(22) Ianni, A.; Waldvogel, S. R. *Synthesis (Stuttg).* **2006**, *2006* (13), 2103–2112.

(23) Tardiff, B. J.; McDonald, R.; Ferguson, M. J.; Stradiotto, M. *J. Org. Chem.* **2012**, *77* (2), 1056–1071.

(24) Ruiz-Castillo, P.; Blackmond, D. G.; Buchwald, S. L. *J. Am. Chem. Soc.* **2015**, *137* (8), 3085–3092.

(25) Green, R. A.; Hartwig, J. F. *Org. Lett.* **2014**, *16* (17), 4388–4391.

(26) Gosselink, R. J. A.; De Jong, E.; Guran, B.; Abächerli, A. In *Industrial Crops and Products*; Elsevier, 2004; Vol. 20, pp 121–129.

(27) Tuck, C. O.; Pérez, E.; Horváth, I. T.; Sheldon, R. A.; Poliakoff, M. *Science* **2012**, *337* (6095), 695–699.

(28) Sanderson, K. *Nature* **2011**, *474* (7352), S12–S14.

(29) Dingerdissen, U.; Martin, A.; Herein, D.; Wernicke, H. J. In *Handbook of Heterogeneous Catalysis*; Wiley-VCH Verlag GmbH & Co. KGaA: Weinheim, Germany, 2008; pp 37–56.

(30) Fujishima, A.; Honda, K. *Nature* **1972**, *238* (5358), 37–38.

(31) Tsukamoto, D.; Shiraishi, Y.; Sugano, Y.; Ichikawa, S.; Tanaka, S.; Hirai, T. *J. Am. Chem. Soc.* **2012**, *134* (14), 6309–6315.

(32) Wen, Y.; Liu, B.; Zeng, W.; Wang, Y. *Nanoscale* **2013**, *5* (20), 9739–9746.

(33) Cheng, H.; Fuku, K.; Kuwahara, Y.; Mori, K.; Yamashita, H. *J. Mater. Chem. A* **2015**, *3* (10), 5244–5258.

2. Alumina as a Cross-Coupling Catalyst

2.1. Background

Although not considered a base metal, Cobalt has received increasing attention over the years as an alternative catalyst in the palladium-dominated realm of catalytic cross-coupling chemistry. Offering a much lower cost to the palladium standard and perhaps unique reactive properties, cobalt salts have been shown to catalyze a myriad of reactions including C-H bond activation, Buchwald-Hartwig couplings and Suzuki couplings.[1–4] In the case of the latter, Cobalt has shown less efficacy toward aryl halide engagements than its group 10 neighbors nickel and palladium but is still feasible nonetheless. Often, a Grignard or other additional organometallic forming agent such as zinc is required for reactivity, especially in the case of the less activated aryl chlorides, due to cobalt's poor activity relationship. The role of the adjunct is to assist in the activation of the aryl halide where the aryl halide bond is not easily dissociated or broken by the cobalt catalyst, typically carried out by the direct insertion of the adjunct metal. This however is not a catalytic action and does incur that at least a stoichiometric amount of metal is required to create the activated species. Grignard reagents are distinctly reactive species and the difficulty in preparing or handling these materials in addition to the waste produced by these Grignards has accordingly not made cobalt the most competitive of metal catalysts in Suzuki coupling when compared to palladium or nickel. What's more, cobalt loadings are quite often high, only going as low as 10 mol% in the best of cases.

Despite this, one published article has claimed to have performed catalytic cross coupling of aryl chlorides without the need for an ancillary organometallic, under ligand free conditions with notably small cobalt loadings. The publication was originally picked up to help establish a baseline in starting a new project on cobalt oxide nanoparticle photo-catalyzed reactions by our group. It would serve to aid in understanding what types of transformations would pair well with the envisioned system. It utilized cobalt oxide immobilized on an aluminum oxide support to catalyze the coupling of aryl chlorides to various amines. However, upon closer examination of the published optimizations and reaction scope, it appeared that important controls and other key test reactions were missing entirely, not even found in the supporting information.

The most significant of these withholdings was a control reaction for activity of the catalyst support alone. It is stated that cobalt is employed at a 5 mol% loading relative to the substrate; however, there is only a small amount of cobalt on the alumina itself, which makes up over 90% of the catalyst by mass. Based on the amount of cobalt present, as determined by AAS, the amount of alumina in any given reaction thereby corresponds to a 20 mol% loading relative to the substrate. Test reactions examining the role of the catalyst either remove it entirely, along with the support, or change the loading of cobalt, presumably by reducing the total amount of catalyst present altogether. Thus, the amount of alumina is changing drastically as the amount of cobalt is changed even slightly. Furthermore, the experimental of the publication only states a single synthesis of the catalyst at a fixed loading of cobalt in addition to only presenting characterization for that specific loading.

These findings began raising a cautionary flag on whether or not the cobalt was sufficiently participating in the reaction. Turning our attention to the scope of the reaction (Table 2.1), it was immediately clear that only strong electron withdrawing groups were used and exclusively in the ortho and para ring positions. In fact, the substrates chosen for the scope are often found in chemistry textbooks as teaching examples for nucleophilic aromatic substitution reactions (S_NAR).[5] Intrigued by this, we entertained the idea that these reactions may not actually be true cross coupling at all. Additionally, no mechanistic data or a plausible catalytic cycle was provided in the paper to argue otherwise.

The placement of these strong electron withdrawing functionalities on the ortho/para ring sites greatly enhances the ability of the ring system to dissipate the excess negative charge brought about by the addition of a nucleophile to the ipso site through the increased resonance capability. It is possible that meta-activated substrates were simply not tried but if S_NAR is responsible for the observed reactivity, these positions would likely greatly hamper the productivity of the reaction. If this reaction followed the cross-coupling convention of the catalyst dissociating the aryl halide bond, the location of electron withdrawing groups should not be as pivotal. A good catalyst operating in this manner will also tolerate many more functionalities including electron neutral and even electron donating (EDG) groups on the ring. If cobalt is not engaging the substrate this way, its role becomes increasingly less clear.

Table 2.1. Published Scope of the Coupling of Aryl Chlorides to Amines. Adapted with permission from Mukherjee *et al.*[6] Copyright 2015 WILEY-VCH Verlag GmbH & Co. KGaA, Weinheim

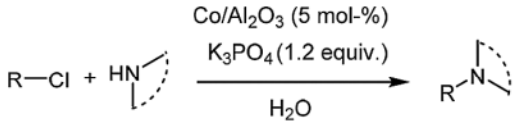

Entry	R	Product	Time [h]	Yield [%][b]	Ref.
1	4-NO_2-C_6H_4-	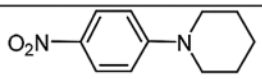	7	87	[11c]
2	4-CN-C_6H_4-	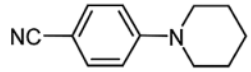	8	86	[16]
3	2-NO_2-C_6H_4-	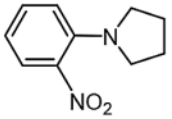	7	87	[11c]
4	2-NO_2-C_6H_4-	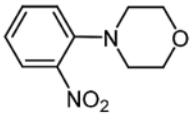	7	90	[17]
5	2-NO_2-C_6H_4-	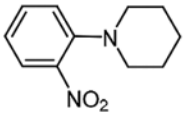	7	90	[18]
6	2-CHO-C_6H_4-	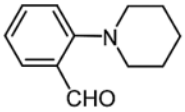	9	79	[19]
7	2,4-diNO_2-C_6H_3	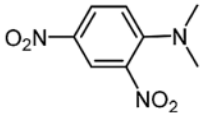	7	94	[20a]
8	4-NO_2-C_6H_4-	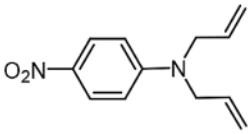	8	77	[20b]
9	4-NO_2-C_6H_4-	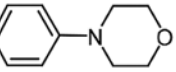	7	90	[11c]
10		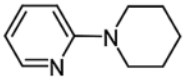	8	83	[11b]
11	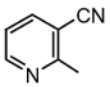	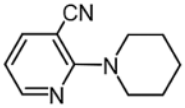	7	92	[21]
12		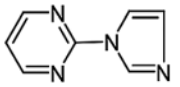	9	90	[22]
13	4-NO_2-C_6H_4-	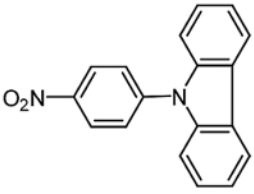	8	83	[23]

To the author's credit, the publication studied the coupling of aryl chlorides. However, the use of a different halide is an easy way to show increased versatility of the system. Typically, aryl halogens bonds become more labile and susceptible to catalytic cleavage as the halogen size increases. This in turn explains why aryl chlorides are less frequently used as coupling partners in cross-coupling chemistry, with many opting to use the more reactive aryl bromides and iodides despite their increased cost. S_NAR reactions follow an opposite trend in reactivity with respect to the halogen present. More electronegative atoms help stabilize the ring system after nucleophilic attack and the aromaticity is broken. This would mean that the use of aryl chlorides is less of an achievement and instead a hard requirement. We predicted that the use of an aryl bromide or iodide in this system would lower productivity.

We decided to probe deeper into the underlying chemistry presented in this publication and perform the experiments we believed to be lacking. Our hope was to achieve similar results to those published without the need for cobalt at all or by using cobalt oxide nanoparticles that could photocatalyze the reaction at room temperature. We further hoped in the case of the former, this reaction could be adapted to use a microwave reactor to further improve its efficiency.

2.2. Results

To establish a baseline, we first attempted to reproduce the protocol described in the publication for an uncatalyzed reaction (Table 2.2, entry 1). Indeed, we achieved a near identical result to those published with 11% yield of the target product without any catalyst present. Next, we tried catalyzing the reaction using naked alumina. We chose neutral activated alumina for this role given the little information on the materials the authors used. Although the reaction did not produce as much of the product as hoped (87%), the catalyst nonetheless improved the yield over the blank by more than a factor of three.

Table 2.2. Control Experiments[a]

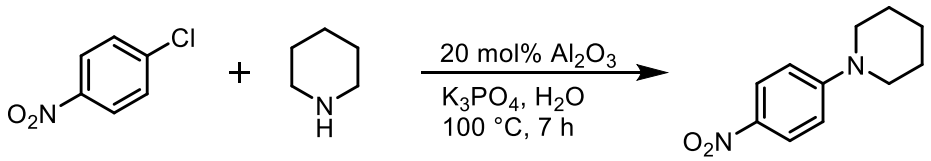

Entry	Deviation	Conversion of Aryl Halide	Yield
1	No Catalyst	18%	11%
2	None	42%	36%
3	4-nitrobromobenzene	6%	trace[b]
4	4-nitroiodobenzene	0%	ND[c]
5	5 mol% Cobalt Oxide NP	16%	10%[d, e]

[a]Reaction conditions: 4-nitrochlorobenzene (1 mmol), piperidine (1.2 mmol), K_3PO_4 (1.2 mmol), Al_2O_3 (20 mol%) dissolved in water (4 mL). Heated with stirring at 100 °C under air for 7 h. [b]4-

nitrobromobenzene used. [c]4-nitroiodobenzene used. [d]Cobalt oxide NP used instead of Al_2O_3 at 100 °C. [e]Cobalt oxide NP irradiated with white light at room temperature. ND: not detected.

Given that alumina clearly had some effect on the reactivity, we decided to replace the activated aryl chloride with an activated aryl bromide and iodide (Table 2.2, entries 3 and 4). As would be expected for an S_NAR reaction, the presence of bromide significantly stunted the reaction yield to produce only a trace of the product with minimal conversion of the starting material. The use of iodide further hampered the system to not produce any measurable amount of product and leave the starting material unchanged. Next, we turned our attention to cobalt, using a previously described method to synthesize cobalt oxide nanoparticles that might catalyze the reaction. When used at a 5 mol% loading and heated, no increase in reactivity was observed beyond that of our control reaction (Table 2.2, entry 5). Switching the energy source from heat to visible light from a solar simulator resulted in no measurable reactivity or conversion of the starting material.

Determined to optimize the reaction, considering the alumina may still prove more effective on its own and without the need for cobalt, we began adjusting reaction conditions. In a general sense, an optimized and efficient cross coupling catalyst would probably not be effected very much by an increase in reactant concentration since it will be self-limited by its turn over frequency (TOF). The turnover frequency acts as a ceiling where a catalytic site can only engage a certain number of molecules in a given period of time. A bimolecular substitution reaction on the other hand, is a second order process and would benefit from increased reaction rates by increasing the concentration of either of its reactants. We therefore performed two trial reactions at

an increased and decreased concentration of reactants to determine the effect of concentration on the system. Lowering the concentration of all components by a factor of approximately 3 reduced the reaction yield and conversion by half (Table 2.3, entry 1). Conversely, raising the concentration by a factor of 10 nearly doubled the productivity, achieving a result much closer to that which was published (Table 2.3, entry 3). Lastly, we doubled the reaction time at the increased concentration (10 mmol scale) and observed a yield that matched the published value without the need for cobalt or any modification of the commercial alumina (Table 2.3, entry 4).

Table 2.3. Effect of Aryl Chloride Concentration in a Cobalt-Free System[a]

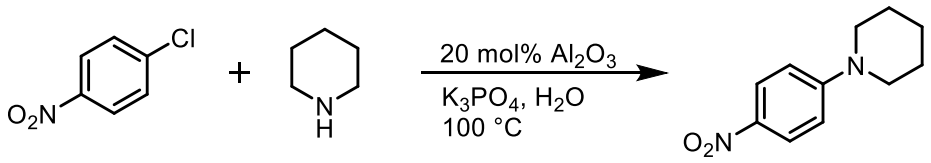

Entry	Concentration	Time	Conversion of Aryl Halide	Yield
1	0.075 M	7 h	20%	18%
2	0.25 M	7 h	42%	36%
3	2.5 M	7 h	64%	64%
4	2.5 M	14 h	87%	87%

[a]Reaction conditions: 4-nitrochlorobenzene (0.3-10 mmol), piperidine (1.2 mmol), K_3PO_4 (1.2 mmol), Al_2O_3 (20 mol%) dissolved in water (4 mL). Heated with stirring at 100 °C under air.

There could be a number of reasons why removing cobalt from the system reduces catalytic activity while naked alumina is only partly effective. Although not thoroughly investigated here, it's plausible that alumina operates as a weak Lewis acid.

These are common catalysts for nucleophilic aromatic substitution reactions as they are thought to lower the energy of the rate limiting transition state. By forming an adduct with the electron saturated complex, alumina acts to stabilize the ring system and dissipate excess negative charge. Modifying the alumina with cobalt could generate stronger Lewis acid sites if not a greater number of them. It is also unclear how different the alumina itself is between the published work and our own, given the lack of information and characterization in the source work.

Published optimizations on the coupling of aryl chlorides showed much better results in polar solvents (Table 2.4, entries 3, 4 and 5). This is an expected result in S_NAR reactions since non polar solvents cannot stabilize the transition state as effectively due to less intermolecular interactions.

Table 2.4. Published Table of Optimizations for the Coupling of Aryl Chlorides to Amines. Adapted with permission from Mukherjee et al.[6] Copyright 2015 WILEY-VCH Verlag GmbH & Co. KGaA, Weinheim

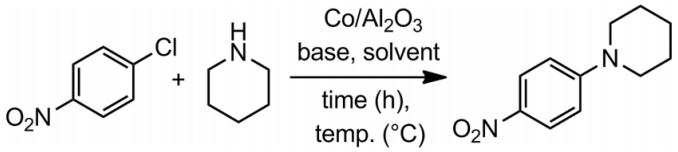

Entry	Base	Solvent	Temp. [°C]	Time [h]	Yield [%][b]
1	K_3PO_4	toluene	100	9	0
2	K_3PO_4	THF	65	9	0
3	K_3PO_4	DMF	120	8	80
4	K_3PO_4	DMSO	120	8	76
5	K_3PO_4	H_2O	100	7	87
6	K_3PO_4	H_2O	80	7	72
7	K_3PO_4	H_2O	80	9	73
8	K_2CO_3	H_2O	100	7	63
9	$KHCO_3$	H_2O	100	7	58
10	$NaHCO_3$	H_2O	100	7	51
11[c]	K_3PO_4	H_2O	100	7	62
12[d]	K_3PO_4	H_2O	100	7	10

[a] Reaction conditions: 1-chloro-4-nitrobenzene (1 mmol), piperidine (1.2 mmol), base (1.2 mmol), Co/Al_2O_3 (5 mol-% of Co), solvent (4 mL). [b] Isolated yields of pure products (by ^1H and ^{13}C NMR spectroscopy). [c] Co/Al_2O_3 corresponding to 3 mol-% of Co was used. [d] Co/Al_2O_3 was not used.

We were interested in observing the effect of raising the reaction system's temperature, to which many common nonpolar solvents are the more suitable option compared to the previously used polar solvents due to their higher boiling points. By raising the temperature, a larger population of molecules will have enough energy to enter the highly unfavorable transition state, allowing the reaction to proceed more rapidly. We chose *para*-xylene as it has a boiling point of 138 °C and indeed the reaction was immediately hindered compared to using water as a solvent (Table 2.5, entry 1), operating about as well as our control reaction without catalyst. An increase in reaction temperature to that of the solvents boiling point and double reaction time were

required to achieve a more suitable yield of 60%, albeit still inferior to the system in aqueous media. We lastly changed our base from tribasic potassium phosphate to sodium bicarbonate which, in non polar media, showed some improvement (Table 2.5, entry 3).

Table 2.5. Alumina Catalyzed Aryl Chloride Substitutions in Xylene[a]

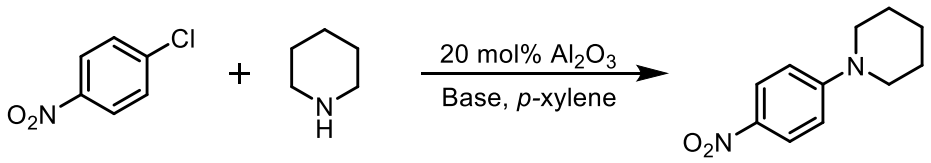

Entry	Temperature	Base	Time	Conversion of Aryl Halide	Yield
1	100 °C	K_3PO_4	7 h	14%	14%
2	140 °C	K_3PO_4	14 h	60%	60%
3	140 °C	$NaHCO_3$	14 h	68%	68%

[a]Reaction conditions: 4-nitrochlorobenzene (1 mmol), piperidine (1.2 mmol), base (1.2 mmol), Al_2O_3 (20 mol%) in *para*-xylene (4 mL). Heated with stirring under air.

Interested in adapting this work to a microwave reactor, we continued our work with naked alumina. Since microwave reactors can be very efficient heaters, our intention was to decrease reaction times while keeping up productivity. We initially tried 1-hour irradiation at 140 °C in *p*-xylene and achieved a modest 34% yield (Scheme 2.1). Yet, it was at this time we discovered a publication reporting very high yields of substitution between many different aryl halides and a very broad scope of nucleophiles, leaving us to abandon the project.[7] These reactions were performed in a microwave reactor without any transition metal catalyst and for irradiation times of only

5 minutes, nonetheless out producing both our work and the original publication we sought to investigate. The main disadvantage to this system was the use of potassium *tert*-butoxide as a necessary base, thus rendering our work as a milder, albeit less efficient alternative.

Scheme 2.1. Microwave Assisted Substitution of 4-Nitrochlorobenzene

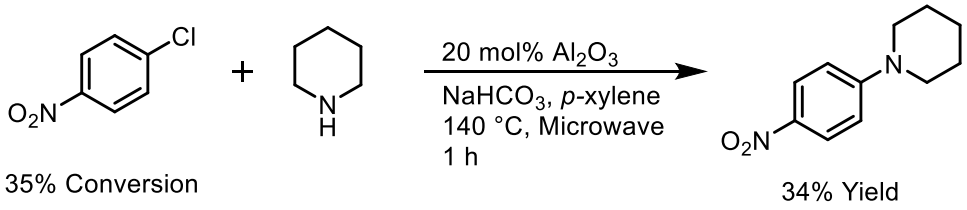

2.3. Conclusion

We have demonstrated that alumina is a capable heterogeneous catalyst in its own right and does not truly require additional post synthetic modification with cobalt to be effective. Additionally, we have uncovered reactivity trends that closely resemble that of nucleophilic aromatic substitution reactions, shedding light on the underlying chemical mechanism. It is plausible that cobalt did not in fact "cross-couple" any aryl halides from a heterogeneous support; instead catalyzing the reaction in some other way. Although inconclusive in this regard, it is plausible the catalyst actually operates by stabilizing the highly energetic transition state of an S_NAR reaction which serves as the rate limiting step.

2.4. Appendix

2.4.A. General Information

Substrates and Reagents: Piperidine, 4-nitrochlorobenzene, 4-nitrobromobenzene, 4-nitroiodobenzene, activated alumina (Brockmann I), potassium phosphate (tribasic), cobalt(II) nitrate hexahydrate, ammonium bicarbonate and *para*-xylene were purchased from Sigma Aldrich or Fisher and used as received without purification.

Microwave Irradiation: Microwave irradiation was performed using a Biotage Initiator Classic microwave reactor.

NMR: All ^{1}H NMR were recorded on a Bruker Avance II 300 spectrometer. Chemical shifts (δ) are reported in ppm from the solvent.

2.4.B. Emission Spectrum of the Solar Simulator

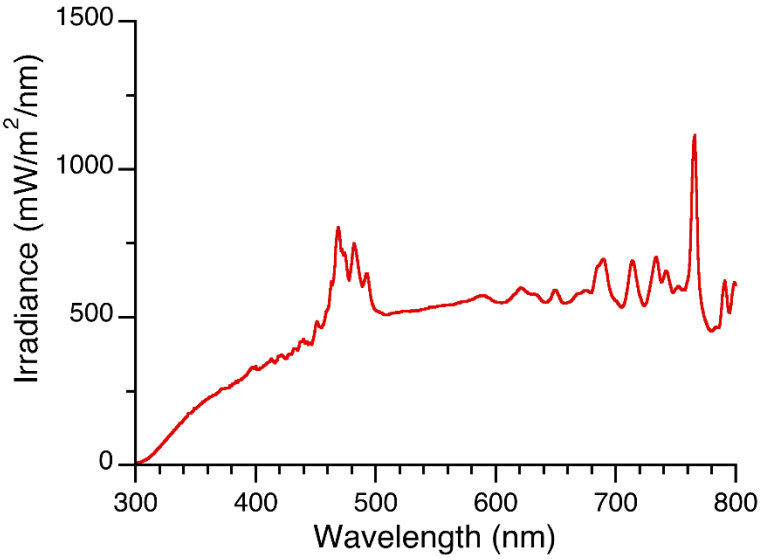

Figure 2A.1. Emission Spectrum of the solar simulator used for irradiation of cobalt oxide nanoparticles.

2.4.C. Diffuse Reflectance Spectrum of Cobalt Oxide Nanoparticles

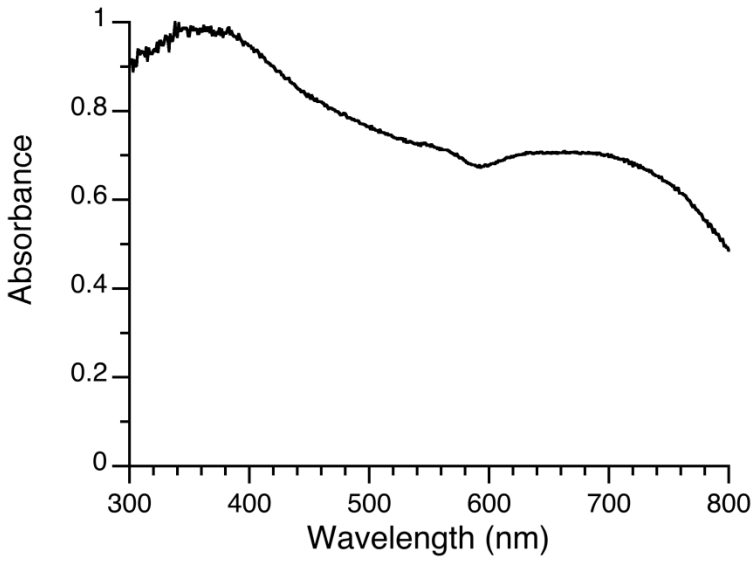

Figure 2A.2. Normalized diffuse reflectance spectrum for cobalt oxide nanoparticles.

2.4.D. General Procedure for the Alumina Catalyzed Substitution of Aryl Halides with Piperidine

The procedure was modeled after a previously published protocol.[6] In a dry 25 mL round bottom flask, 4-nitrochlorobenzene (157 mg, 1 mmol), Al_2O_3 (20 mg) and K_3PO_4 (254 mg, 1.2 mmol) were combined along with a magnetic stir bar. Piperidine (118 µL, 1.2 mmol) was then added via micro syringe and the resulting mixture dissolved in water (4 mL). The round bottom flask was fitted with a condenser and heated to 100 °C in an oil bath under air for 7 h. Upon completion, the catalyst was filtered out of the crude reaction mixture and the filtrate washed with ethyl acetate (4 x 15 mL). The extract was then washed with water and brine before drying over anhydrous $MgSO_4$. The dried liquid was filtered and the remaining $MgSO_4$ washed with fresh ethyl acetate. The solvent was evaporated on a rotary evaporator to produce a pale-yellow residue and further dried under high vacuum for one hour.

2.4.E. General Procedure for the Microwave Assisted Substitution of Aryl Halides with Piperidine

In a 10 mL microwave tube, 4-Nitrochlorobenzene (1.57 g, 10 mmol), Al_2O_3 (200 mg) and K_3PO_4 (2.54 g, 12 mmol) were combined along with a magnetic stir bar. Piperidine (1.2 mL, 12 mmol) was then added via syringe and the resulting mixture dissolved in *para*-xylene (3 mL) to reach a total volume of approximately 4 mL. The microwave tube was covered with a Teflon seal and secured tightly with an aluminum crimp cap. The tube was then placed in an automated Biotage Initiator Classic microwave reactor and irradiated for 1 h at 140 °C. Upon completion, the catalyst was filtered out of the crude reaction mixture and the filtrate evaporated on a rotary evaporator to produce a pale-yellow residue. The product was further dried under high vacuum for one hour.

<u>1-(4-nitrophenyl)piperidine</u> [Table 2.2, entry 4]

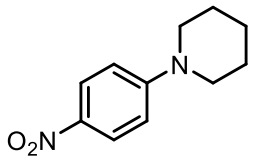

Prepared according to the general procedure, Piperidine (1.2 mL, 12 mmol), 4-Nitrochlorobenzene (1.57 g, 10 mmol), Al_2O_3 (200 mg) and K_3PO_4 (2.54 g, 12 mmol) in water (4 mL) afforded the title compound as a pale yellow solid (Concentrated yield = 87%)

^{1}H NMR (chloroform-d, 300 MHz): δ = 8.18 (d, *J*=9.6 Hz, 2 H), 6.82 (d, *J*=9.6 Hz, 2 H), 3.48 (s, 4 H), 1.76 ppm (s, 6 H)

2.4.F. General Procedure for the Synthesis of Cobalt Oxide Nanoparticles

The procedure was modeled after a previously published protocol.[8] Cobalt(II) nitrate hexahydrate (582 mg, 2 mmol) was mixed in a 2:5 molar ratio with ammonium bicarbonate (395 mg, 5 mmol) in an agate mortar and pestle. At room temperature, the two solids were mixed and milled to quickly produce a purple foamy paste releasing ammonia and carbon dioxide. The color of the composition changed regularly while it was milled for 30 minutes, finally producing a grey solid with no more color changes. The solid was then washed with distilled water (5 x 20 mL), transferred to a ceramic crucible and left to dry in air at 100 °C to produce the nanoparticle precursor. After drying, the precursor was calcined under air at 300 °C for 2 h to obtain the cobalt oxide nanoparticles as a fine black powder.

2.4.G. NMR Data

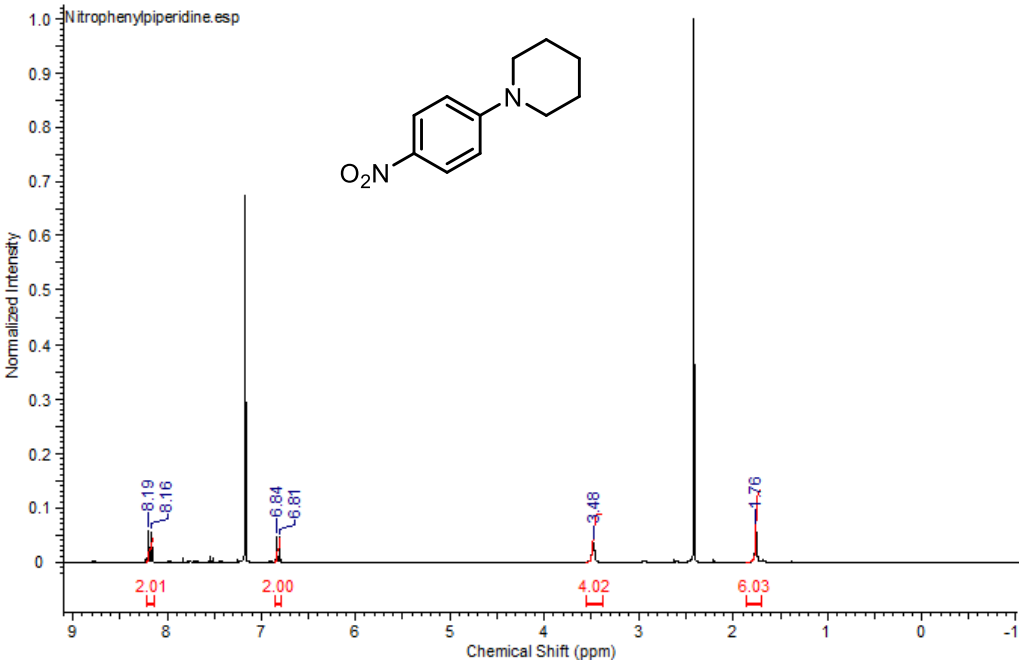

Figure 2A.3. ^{1}H NMR of **product 1** in $CDCl_3$

2.5. References

(1) Cahiez, G.; Moyeux, A. *Chem. Rev.* **2010**, *110* (3), 1435–1462.

(2) Snyder, N. L.; Medici, E. J. *C-H Bond Act. Org. Synth.* **2015**, *6* (2), 217–250.

(3) Gosmini, C.; Bégouin, J. M.; Moncomble, A. *Chem. Commun.* **2008**, No. 28, 3221–3233.

(4) Gosmini, C.; Moncomble, A. *Isr. J. Chem.* **2010**, *50* (5–6), 568–576.

(5) Wade, L. G. *Organic Chemistry*, 6th ed.; Pearson Prentice Hall: Upper Saddle River, 2006.

(6) Mukherjee, N.; Chatterjee, T.; Ranu, B. C. *Eur. J. Org. Chem.* **2015**, *2015* (18), 4018–4023.

(7) Shi, L.; Wang, M.; Fan, C. A.; Zhang, F. M.; Tu, Y. Q. *Org. Lett.* **2003**, *5* (19), 3515–3517.

(8) Yang, H.; Hu, Y.; Zhang, X.; Qiu, G. *Mater. Lett.* **2004**, *58* (3–4), 387–389.

3. Light-Mediated C-H Arylations Utilizing a Nickel Photoredox Catalyst

3.1. Background

Photoredox catalysis has been gaining traction as an alternative to thermally driven reactions due to its compatibility with mild conditions for substrate activation. Commonplace in these systems are ruthenium- and iridium-based complexes which are used as photosensitizers, given their long excited state lifetimes and robust character. These catalysts however, suffer from high costs (some up to $1700/g) and may still require an additional noble metal catalyst to enable cross-coupling reactions. Therefore, the development of lower cost or multifunctional catalysts is desirable to further develop this field and increase industrial relevance.

Furthermore, the facile formation of carbon-carbon bonds has always been a much sought-after process in organic synthesis. Although carbon-carbon bond forming reactions have existed for over a century, it was not until the late 1970's that most modern catalytic C-C coupling reactions were developed.[1–6] These new systems enabled C-C bonds to be formed between vast numbers of diverse coupling partners, typically employing much milder conditions, cheaper, more available reagents and only using minute amounts of catalytic material. Many of the strategies used to perform these coupling reactions employed the use of palladium-based catalysts which, though effective, are still very expensive. A large component of current research in this field is therefore in finding suitable base metal alternatives to these noble metal catalysts.

In recent years, the synergistic relationship between photoredox and transition metal catalysis has demonstrated new avenues for the coupling of non-traditional partners. Recent works have shown that alkyl radicals generated from single-electron transfer (SET) events could be effectively intercepted by Ni(I) and Ni(II) complexes that, when in conjunction with another coupling partner afford a productive heterocoupling reaction.[7–9] Additionally, the use of boronic acids allows for facile redox neutral transmetalation in the presence of base, tolerant of various common nickel oxidation states. The convergence of these two systems could afford a Ni(II) or Ni(III) intermediate, capable of undergoing reductive elimination to furnish the desired cross coupled product. The potential scopes of these systems are large but generally only require tuning of the photocatalyst redox potentials to adapt the system to new substrates.

We envisioned a dual catalytic system using the ubiquitous semiconductor TiO_2 as a replacement photocatalyst to the common series of iridium complexes currently used. Upon photoexcitation, electrons from the conduction band would reduce the peroxide to a *t*-butoxy radical and *t*-butoxide anion.[10] The radical would subsequently abstract hydrogen from the α-carbon of the ether, generating a carbon centered alkyl radical. After binding to the active Ni(II) complex, transmetalation would occur before a reductive elimination step generating an electron rich Ni(I) species. The highly oxidizing hole of the semiconductor VB could accept an electron from the metal, turning over the cycle and regenerating the active Ni(II) state. A proposed mechanism for the TiO_2/Ni photoredox catalysis is shown in Scheme 2.1.

Scheme 3.1. Proposed Mechanism for the TiO_2/Ni Photoredox Mediated C-H Arylations

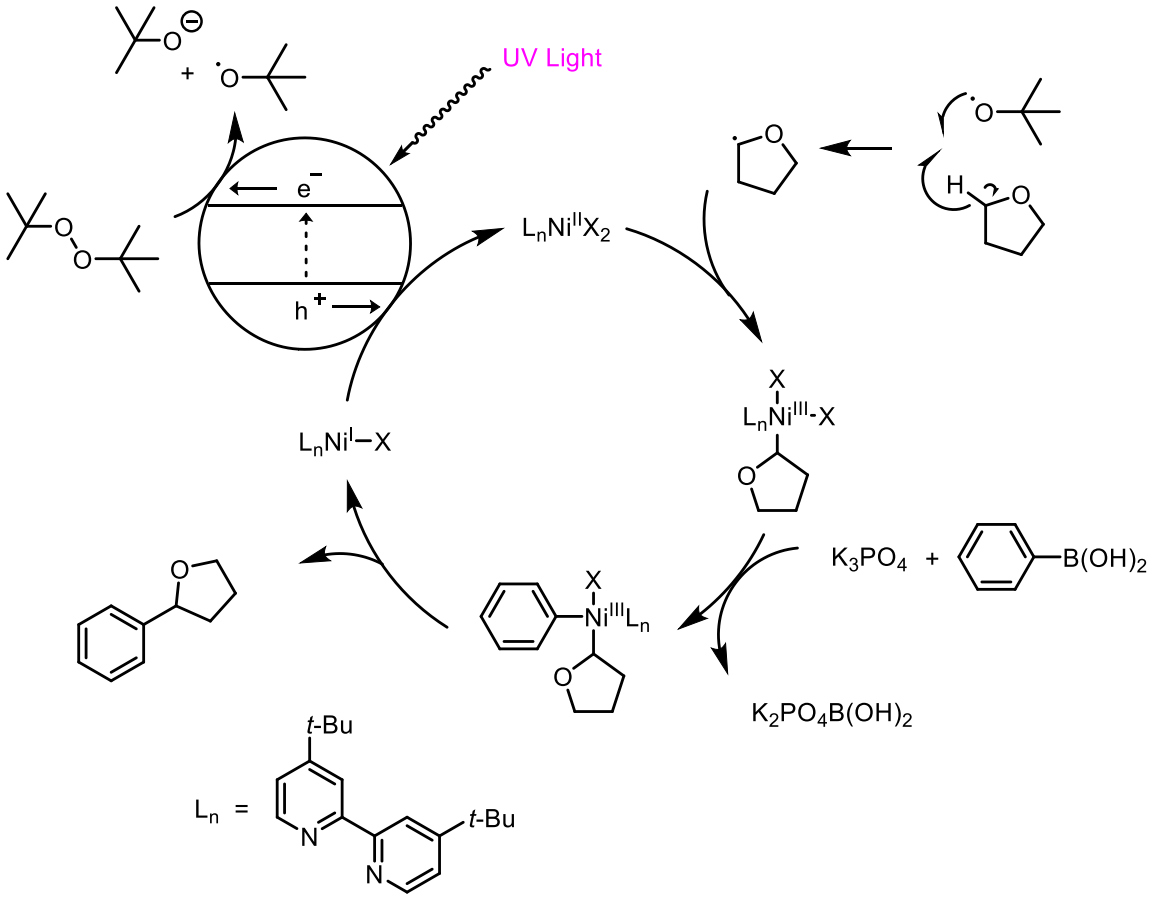

3.2. Optimization and Controls

Optimization of the C-H arylations began using an iridium complex and P25 TiO_2 as photoredox catalysts, a number of nickel-based catalysts, Cs_2CO_3 as base, di-tert-butyl peroxide as a precursor reducing agent and a UVA-visible light source for sample irradiation (Luzchem Inc. Solar Simulator). Phenylboronic acid was selected as a model coupling partner for the arylation of THF, used both as solvent and reagent in the system. Test and control reactions were carried out under several different conditions to optimize the procedure.

Table 3.1. Optimization of Reaction Conditions and Control Reactions[a]

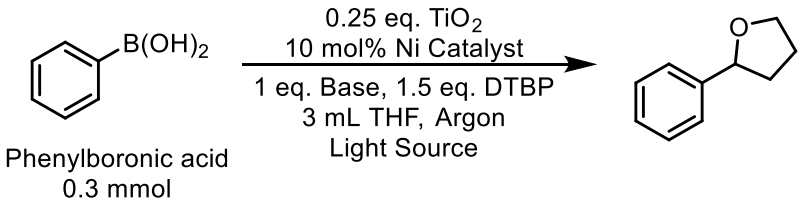

Entry	Photocatalyst	Nickel Catalyst	Base	Yield
1	$Ir(ppy)_3$	$NiCl_2$(dtbbpy)	Cs_2CO_3	30%[b]
2	TiO_2	$NiCl_2$(dtbbpy)	Cs_2CO_3	35%[c]
3	$Ir(ppy)_3$	$NiCl_2$(dtbbpy)	K_2CO_3	63%[b]
4	TiO_2	$NiCl_2$(dtbbpy)	K_2CO_3	55%
5	TiO_2	$NiCl_2$(dtbbpy)	K_2HPO_4	37%
6	TiO_2	$NiCl_2$(dtbbpy)	K_3PO_4	73%
7	None	$NiCl_2$(dtbbpy)	K_3PO_4	>95%
8	None	$NiCl_2$(dtbbpy)	None	ND
9	None	None	K_3PO_4	ND
10	None	$NiCl_2$(dtbbpy)	K_3PO_4	ND[d]
11	None	$NiCl_2$(glyme)	K_3PO_4	trace
12	None	$Ni(acac)_2$	K_3PO_4	trace
13	None	$NiCl_2(PPh_3)_2$	K_3PO_4	trace
14	None	$NiCl_2$(dtbbpy)	K_3PO_4	trace[e]
15	$Ni@TiO_2$	None	K_3PO_4	ND[a,b,c]
16	$Pd@TiO_2$	None	K_3PO_4	ND[a,b,c]
17	TiO_2	None	K_3PO_4	ND[a,c]

[a]Reaction conditions: Phenylboronic acid (0.3 mmol), base (0.3 mmol), di-tert-butyl peroxide (0.45 mmol), tetrahydrofuran (3 mL). Irradiated with solar simulator for 20 h. [b]LED centered at 465 nm, 1 mol% PC used. [c]LED centered at 368 nm. [d]No di-tert-butyl peroxide. [e]No light. ND: not detected.

Investigation of $Ir(ppy)_3$ and TiO_2 as photocatalysts showed comparable results when irradiated at their lowest energy excitation maxima (465 nm and 358 nm respectively), achieving yields of 30-35% (Table 3.1, entries 1 and 2). After improving yields by selecting K_2CO_3 as a more appropriate base, TiO_2 and solar simulated irradiation were chosen for further work due to their ubiquity and significantly lower cost over iridium-based complexes and LED illumination (Table 3.1, entry 4). Examination of the literature showed widespread use of K_2HPO_4 or K_3PO_4 as base in boronic acid containing catalytic systems, the latter proving to be an effective improvement to our own arylations, improving the yield to 73% (Table 3.1, entry 6). The reduced performance of K_2HPO_4 may be attributed to its lower basicity compared to its tribasic counterpart. It has also been suggested that K_3PO_4 is not just a spectator but plays a direct role in boronic acid activation and transmetalation.[11]

Omission of nickel catalyst, base, DTBP or light resulted in no product or conversion of starting materials after 20 hours of visible light irradiation, demonstrating their necessity in this system (Table 3.1, entries 8, 9, 10 and 14). However, to our surprise, it was later learned that the omission of photocatalyst had the effect of increasing the absolute productivity of the system, increasing the yield to over 95% (Table 3.1, entry 7). The addition of TiO_2 produces milky and blanched reaction mixtures that are highly opaque. The increased performance in the absence of TiO_2 likely can be attributed to the large amount of light scattering inherent to the material after it is dispersed in solution. This would suggest that another material within the system is in fact absorbing the light that is responsible for the photochemistry and is rendered

inefficient by the addition of TiO_2. Interestingly, switching to another Ni(II) ether soluble complex or omitting the dtbbpy ligand also only produces a trace amount of the desired product under otherwise standard conditions (Table 3.1, entries 11, 12 and 13). It should be noted that the use of metals on heterogeneous supports was also ineffective at carrying out the C-H arylations (Table 3.1, entries 15 and 16).

3.3. Phenylboronic Acid Scope

After optimizations were complete, our model system was applied to a variety of phenylboronic acids to determine its utility in a range of diverse cross-coupling partners.

Table 3.2. Nickel Photoredox Mediated C-H Arylations: Scope of Boronic Acids[a]

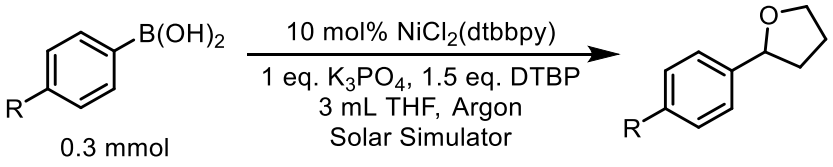

Entry	Boronic Acid	Product	Yield
1	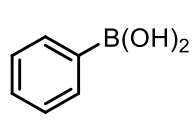	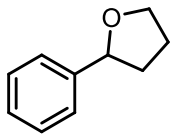	>95%
2	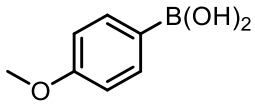	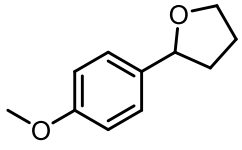	88%
3	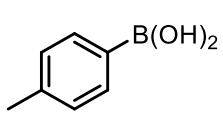	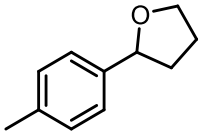	92%

4	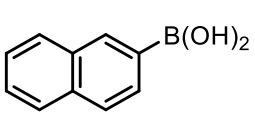	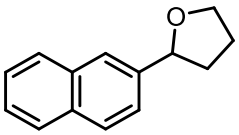	71%
5	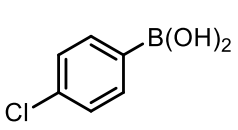	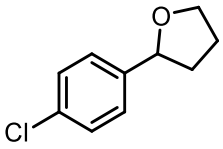	60%
6	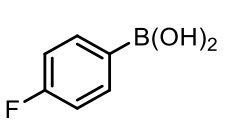	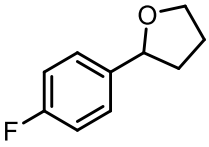	84%
7	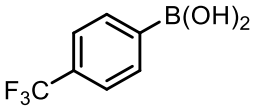	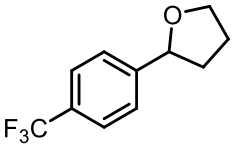	51%[b]
8	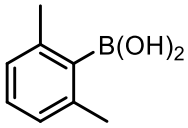	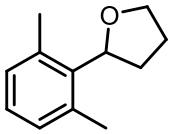	20%

[a]Reaction conditions: Boronic acid (0.3 mmol), K_3PO_4 (0.3 mmol), di-tert-butyl peroxide (0.45 mmol), tetrahydrofuran (3 mL). Irradiated with solar simulator for 20 h. [b]Irradiated for 40 h.

Our model system was effective in coupling electron deficient, neutral and rich phenylboronic acids with good yields (60-95%) under mild conditions and a generally short illumination time of 20 h compared to what is reported in the literature using focused LEDs (24-72 h).[7,9,12–16] Good tolerance was shown for alkoxy, alkyl and halogenated substrates however, the reaction was terminated when carboxylic acid or nitro functionalities were used. This is likely due to the radical trapping nature of nitro groups which would prevent radical hydrogen abstraction from the ether. The carboxylic acid simply salted out and produced a heterogeneous sludge in the reaction mixture; trace deboronated carboxylic acid (benzoic acid) was detected by NMR. Bulky 2-napthylboronic acid coupled quite effectively to afford product 4, however 2,6-

dimethylphenylboronic acid much less so. This low yield shows significantly reduced efficiency for molecules with strong steric interactions around the intended coupling site. The installation of a trifluoromethyl group on the C_4 position of the aromatic ring greatly lowered the solubility of the corresponding boronic acid in THF, likely leading to the observed poor activity, yielding only 21% of the target product under standard conditions. A longer irradiation time of 40 h was required to achieve a more adequate yield of 51%.

In all cases presented in table 3.2, few side products and complete consumption of boronic acid were observed. Typically, biphenyl is the only major side product of the reaction, although the (R) and (S) diastereomers of a THF dimer could be detected in trace amounts via GC-MS and suggest the presence of free THF radicals in the system. The removal of butylated hydroxytoluene (used as stabilizer to prevent autoxidation in ethers and peroxides) from all ethereal solvents and DTBP was found to have no measurable effect on the reactivity of the system. A small amount could still be detected from the solvent post reaction, indicating this radical control agent did not offer significant interference with the system. The removal of water was however, a major factor in the performance of the reaction, improper drying of the base and especially the solvent was found to lower the yield of all products considerably. The addition of 10 µL of distilled water pre-reaction was used to confirm that water was in fact causing this effect, leading to an almost complete shutdown of productivity.

3.4. Scope of Other C(sp^3)-H Bond Arylations

Next, we turned our attention to various aliphatic substrates to determine the applicability of the system toward other C(sp^3)-H bonds. 1,4-dioxane and 1,3-dioxolane coupled with good yields at 80% and 80% respectively (Table 3.3, entries 1 and 2). Increased steric effects coupled with an increased C-H bond dissociation energy (BDE) could explain the lower yield from 1,4-dioxane compared to THF. 1,3-dioxolane was little better in forming our desired product, instead also producing a secondary coupling product resulting from reactivity on the C4 and C5 ring positions. Overall nearly 100% of the boronic acid was consumed to produce one of these two products in a 4:1 ratio. When 1,3-benzodioxole was used, a common moiety in pharmaceutical products, 52% of the desired product was produced (Table 3.3, entry 3). Furthermore, it was discovered that in addition to C(sp^3)-H bonds adjacent to oxygen atoms, those adjacent to nitrogen atoms could also be arylated successfully as we observed on two model amines. *N*,*N*-dimethylaniline coupled particularly well under our optimized reaction conditions affording the desired product in 92% yield (Table 3.3, entry 4). Subsequently, *N*,*N*-dimethylacetamide which is a commonly used polar aprotic solvent, mono arylated moderately well to yield 57% of the target product (Table 3.3, entry 5).

Table 3.3. Nickel Photoredox Mediated C-H Arylations: Scope of Other C(sp^3)-H Bonds[a]

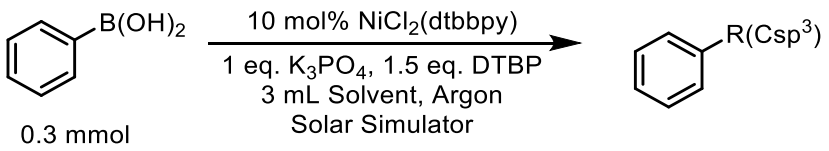

Entry	Substrate	Product	Yield
1	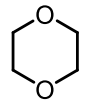	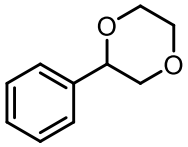	80%
2		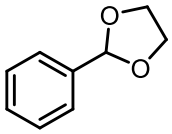	80%
3	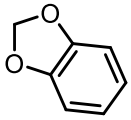	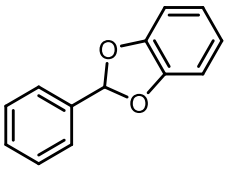	52%
4	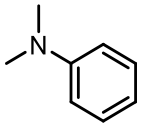	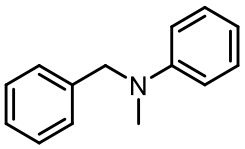	92%
5		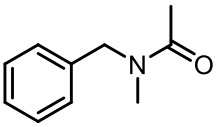	57%

[a]Reaction conditions: Phenylboronic acid (0.3 mmol), K_3PO_4 (0.3 mmol), di-tert-butyl peroxide (0.45 mmol), coupling partner (3 mL). Irradiated with solar simulator for 20 h.

3.5. Mechanistic Insights

Scheme 3.2 depicts a plausible mechanism for the Nickel catalyzed C-H arylations with boronic acids. Initially, potassium phosphate may generate a Ni(0) complex through the irreversible precipitation of KCl in an activation step. This low valent nickel species may then operate as a pseudo Fenton reagent, performing a single electron reduction of

the peroxide and generating a Ni(I) intermediate. The ensuing ^{t}butoxy radical would be a good candidate for the radical abstraction of hydrogen from THF, given its high relative concentration. The Nickel complex would then intercept the THF radical to form the more stable Ni(II) complex before transmetalating with the boronic acid. The transmetalation step can also be greatly accelerated by the in situ activation of the boronic acid with ^{t}butoxide ions, providing the much more reactive boronate anion. The cycle would turnover with the reductive elimination of the product and regeneration of the Ni(0) complex. Elimination can be expected to occur through an associative mechanism from a square planar complex whereby a ligand such as THF or phosphate bond to nickel and form a five-coordinate complex. A photon may be utilized at this stage to favor the elimination of the product from the Ni(II) species.

Scheme 3.2. Proposed Mechanism for the Ni Photoredox Mediated C-H Arylations

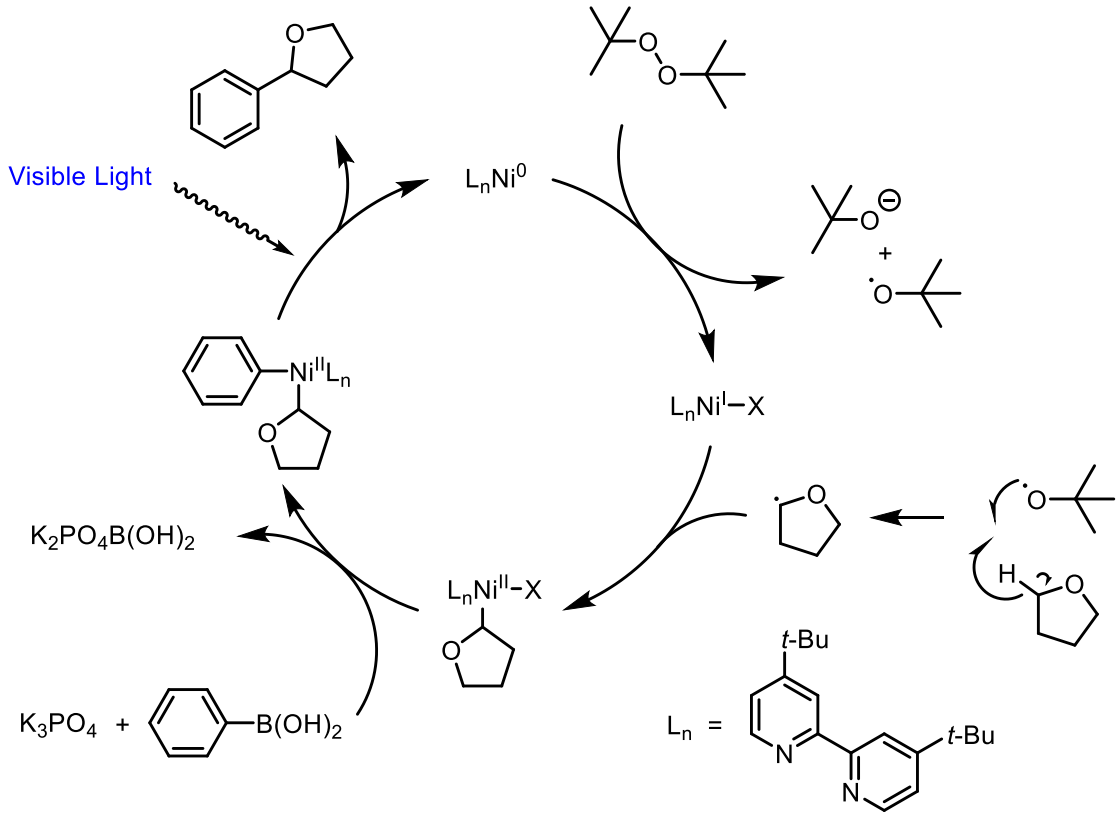

The only species present that absorbs visible light is the Nickel complex, suggesting that any photochemistry is a result of this species. Centrifugation of the reaction mixture yields a transparent, red colored solution and isolates the insoluble base which remains white. Celite filtration of the resulting solution, which removes metal species, dissipates all color from the reaction mixture and 100% mass balance can be observed of the remaining organics in solution by NMR. UV-VIS spectroscopy of $NiCl_2$(dtbbpy) in THF shows strong absorption features in the UVA/near-visible region corresponding largely to the ligand (Figure 3.1). Another absorption maximum is present at 420 nm in addition to a broad absorption band starting at 530 nm, extending into the

NIR range. However, absorption spectra of the reaction mixture after formation of the red nickel complex reveal a broad absorption band centered at 465 nm.

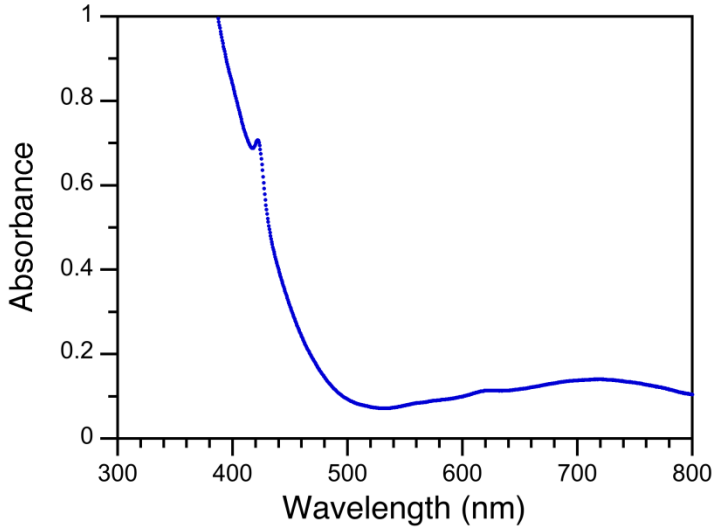

Figure 3.1. Absorption profile of 10 mM $NiCl_2$(dtbbpy) in THF.

To get a better idea of the photochemistry at hand, the reaction mixture was allowed to settle until the solution was no longer opaque from the suspension of base. An aliquot of the mixture was diluted in a sealed quartz cuvette and purged with argon. This sample was then irradiated under standard reaction conditions for 5-minute intervals whereby the red color of the mixture would progressively disappear and then later reappear when allowed to sit in the dark (Figure 3.2). This suggests that a nickel intermediate may be using visible light to turn over the cycle. Due to difficulty isolating and analyzing the nickel intermediate, it is difficult to know the true structure of this complex. The color change does however hint that the nickel complex is either oxidized to a higher oxidation state or has ligands within its coordination sphere that have a stronger field effect than a chloride ligand. Both of these scenarios would increase the splitting of the non-degenerate d-orbitals participating in bonding, resulting in a larger energy difference and blue shift of the absorption.

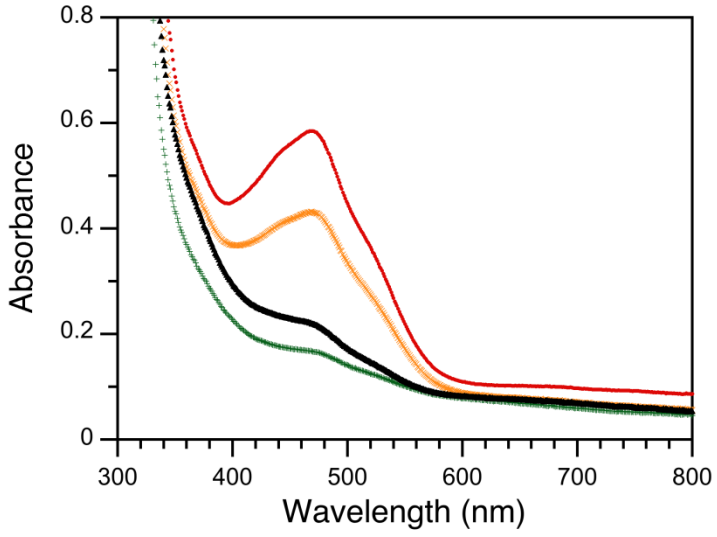

Figure 3.2. Absorption spectra of the reaction supernatant for the nickel catalyzed coupling of phenylboronic acid in THF, diluted by a factor of 6, with no irradiation (•), 5 minutes irradiation (x), 10 minutes irradiation (+) and 10 minutes of darkness immediately following irradiation (▲).

Even when subjected to UVB irradiation in the presence of TiO_2, which absorbs strongly in this region, no product is formed and indeed very little boronic acid is consumed (Scheme 3.3). The peroxide is also a moderately strong absorber in this region and should cleave rapidly under these conditions but perhaps decomposes too quickly to be an effective hydrogen abstracter. The solution quickly becomes an intense violet color which immediately disappears on contact with atmosphere, possibly from the formation of fully reduced Ni(0) which is quickly oxidized in air.

Scheme 3.3. UVB Irradiation of TiO_2/Nickel System

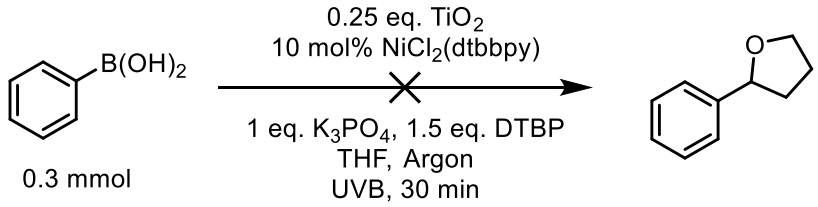

The failure of Nickel supported on titanium dioxide to be a productive catalyst and the requirement of the dtbbpy ligand implies that the Nickel complex may need to be allowed to readily switch oxidation states and also act as an anchor to reactive species in solution such as the THF radical. This bipyridyl ligand may be the only one capable of stabilizing the metal to a high enough degree to achieve this effect in addition to solubilizing the complex. An alternative explanation for the necessity of this ligand is in the photophysical properties of the catalyst, the dtbbpy ligand may allow for proper absorption of light in the complex and MLCT events to occur, making the catalyst act in the same mode as a ruthenium bipyridyl complex, for example.

3.6. Conclusion

We have developed an efficient photoredox system that is capable of performing photochemistry without the need for an ancillary photosensitizer as is seen in most dual photoredox systems, instead utilizing a low-cost nickel complex to promote reactivity. The implementation of boronic acids as a substrate in conjunction with solar simulated illumination as the primary energy source of the reaction further enables mild reaction conditions and efficient coupling using low cost materials.

3.7. Appendix

3.7.A. General Information

Substrates and Reagents: $NiCl_2$(glyme), $Ni(acac)_2$, 4,4'-Di-tert-butyl-2,2'-dipyridyl, P25 TiO_2, triphenylphosphine, benzophenone, all bases and substrates were purchased from commercial suppliers (Sigma Aldrich, Alfa Aesar, Strem and Fisher) and used as received with no purification. Di-tert-butyl peroxide was obtained from Sigma Aldrich and ran through a short column of activated acidic alumina before use to remove any stabilizers or hydroperoxides. All solvents were obtained from a solvent purification system, run through a column of activated acidic alumina to remove stabilizers and then dried for 72 hours over activated 3Å sieves before use.

Light Sources: Solar illumination was performed using a Luzchem Inc. solar simulator operating at 12,200 mW/m^2 UV and 231,800 mW/m^2 visible light power intensity.

NMR: All ^1H NMR were recorded on a Bruker Avance 400 spectrometer. Chemical shifts (δ) are reported in ppm from the solvent.

3.7.B. Absorbance Spectrum of the Nickel Catalyst and Ligand

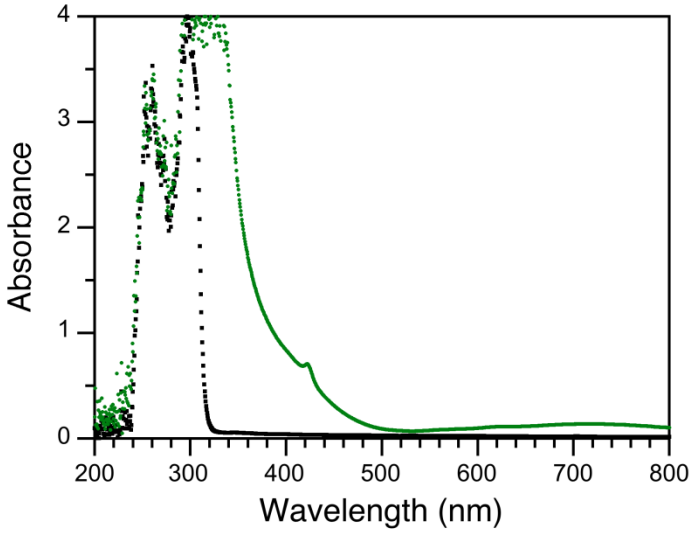

Figure 3A.1. Absorbance spectrum of 10 mM 4,4'-Di-tert-butyl-2,2'-dipyridyl (▪) and 10 mM $NiCl_2$(dtbbpy) (•)

3.7.C. Emission Spectrum of the Solar Simulator

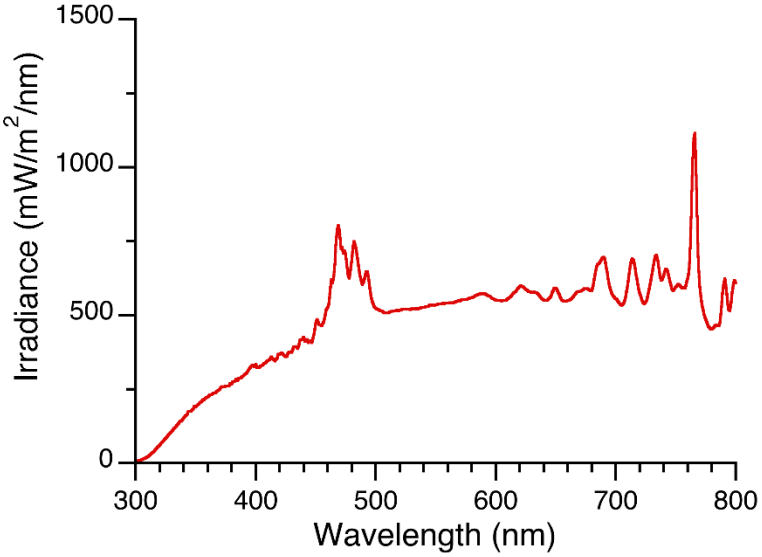

Figure 3A.2. Emission Spectrum of the solar simulator used for irradiation of reaction mixtures.

3.7.D. General Procedure for the Nickel Catalyzed Cross-Coupling of Phenylboronic Acid and THF

An oven dried 10 mL Schlenk flask was quickly charged with 6.6 mg of $NiCl_2$(glyme) and 8 mg of 4,4'-di-tert-butyl-2,2'-dipyridyl before dissolution with 3.0 mL of THF via syringe. The solution was then heated to a boil with a heat gun, until the complex completely dissolved and the solution turned dark green. The flask was then placed on a rotary evaporator and allowed to dry under vacuum to produce light green crystals. After evaporation, the phenylboronic acid derivative (0.3 mmol), K_3PO_4 (64 mg, 0.3 mmol) and 3.0 mL of THF were quickly added to the flask along with a magnetic stir bar and capped with a rubber septum. The solution was purged under argon for 15 minutes before lastly adding di-tert-butyl peroxide (82 µL, 0.45 mmol) via micro syringe and sonicating until no more solids were visible settling at the bottom of the flask (about one minute). The mixture was irradiated by a solar simulator for 20 hours while stirring at room temperature at an angle of approximately 30°. The catalyst, base and borates were separated by filtering the crude mixture through a short pad of Celite under reduced pressure into a round bottom flask. The remaining clear liquid was concentrated under reduced pressure on a rotary evaporator.

<u>2-Phenyltetrahydrofuran</u> [Table 3.2, entry 1]

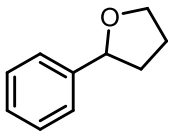

Prepared according to the general procedure, phenylboronic acid (37 mg, 0.3 mmol), K_3PO_4 (64 mg, 0.3 mmol), $NiCl_2$(dtbbpy) (10 mol%), di-tert-butyl peroxide (82 µL, 0.45 mmol) in THF (3 mL) afforded the title compound as a colorless liquid (Concentrated yield = >95%)

^{1}H NMR (chloroform-d, 400 MHz): δ = 7.34 (d, *J*=4.3 Hz, 4 H), 7.23 - 7.28 (m, 1 H), 4.90 (t, *J*=7.3 Hz, 1 H), 4.10 (q, *J*=7.1 Hz, 1 H), 3.94 (q, *J*=7.4 Hz, 1 H), 2.33 (dq, *J*=12.5, 6.4 Hz, 1 H), 1.96 - 2.08 (m, 2 H), 1.76 - 1.87 ppm (m, 1 H)

2-(4-Methoxyphenyl)tetrahydrofuran [Table 3.2, entry 2]

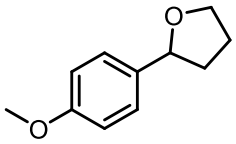

Prepared according to the general procedure, 4-methoxyphenylboronic acid (46 mg, 0.3 mmol), K_3PO_4 (64 mg, 0.3 mmol), $NiCl_2$(dtbbpy) (10 mol%), di-tert-butyl peroxide (82 µL, 0.45 mmol) in THF (3 mL) afforded the title compound as a colorless liquid (Concentrated yield = 88%)

^{1}H NMR (chloroform-d, 400 MHz): δ = 7.26 (d, *J*=8.6 Hz, 2 H), 6.87 (d, *J*=8.8 Hz, 2 H), 4.83 (t, *J*=7.2 Hz, 1 H), 4.05 - 4.12 (m, 1 H), 3.88 - 3.94 (m, 2 H), 3.80 (s, 3 H), 2.23 - 2.32 (m, 1 H), 1.94 - 2.07 (m, 2 H), 1.74 - 1.85 ppm (m, 1 H)

2-(4-Tolyl)tetrahydrofuran [Table 3.2, entry 3]

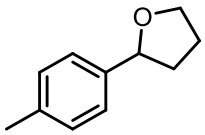

Prepared according to the general procedure, *p*-tolylboronic acid (41 mg, 0.3 mmol), K_3PO_4 (64 mg, 0.3 mmol), $NiCl_2$(dtbbpy) (10 mol%), di-tert-butyl peroxide (82 µL, 0.45 mmol) in THF (3 mL) afforded the title compound as a colorless liquid (Concentrated yield = 92%)

^{1}H NMR (chloroform-d, 400 MHz): δ = 7.19 - 7.25 (m, *J*=8.0 Hz, 2 H), 7.11 - 7.17 (m, *J*=7.8 Hz, 2 H), 4.86 (t, *J*=7.3 Hz, 1 H), 4.05 - 4.13 (m, 1 H), 3.87 - 3.97 (m, 1 H), 2.34 (s, 3 H), 2.25 - 2.30 (m, 1 H), 1.94 - 2.06 (m, 2 H), 1.74 - 1.84 ppm (m, 1 H)

2-(Naphthalen-2-yl)tetrahydrofuran [Table 3.2, entry 4]

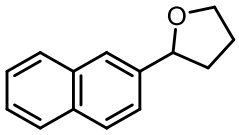

Prepared according to the general procedure, 2-napthylboronic acid (52 mg, 0.3 mmol), K_3PO_4 (64 mg, 0.3 mmol), $NiCl_2$(dtbbpy) (10 mol%), di-tert-butyl peroxide (82 µL, 0.45 mmol) in THF (3 mL) afforded the title compound as a colorless liquid (Concentrated yield = 71%)

^{1}H NMR (chloroform-d, 400 MHz): δ = 7.79 - 7.84 (m, 4 H), 7.41 - 7.48 (m, 3 H), 5.07 (t, *J*=7.2 Hz, 1 H), 4.14 - 4.22 (m, 1 H), 3.97 - 4.05 (m, 1 H), 2.40 (td, *J*=12.4, 7.0 Hz, 1 H), 1.99 - 2.12 (m, 2 H), 1.84 - 1.94 ppm (m, 1 H)

2-(4-Chlorophenyl)tetrahydrofuran [Table 3.2, entry 5]

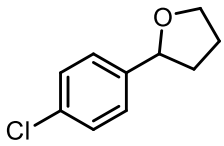

Prepared according to the general procedure, 4-chlorophenylboronic acid (47 mg, 0.3 mmol), K_3PO_4 (64 mg, 0.3 mmol), $NiCl_2$(dtbbpy) (10 mol%), di-tert-butyl peroxide (82 µL, 0.45 mmol) in THF (3 mL) afforded the title compound as a colorless liquid (Concentrated yield = 60%)

^{1}H NMR (chloroform-d, 400 MHz): δ = 7.24 - 7.31 (m, 5 H), 4.86 (t, *J*=7.1 Hz, 1 H), 4.04 - 4.13 (m, 1 H), 3.93 (q, *J*=7.3 Hz, 1 H), 2.27 - 2.36 (m, 1 H), 2.00 (quin, *J*=7.1 Hz, 2 H), 1.75 ppm (dq, *J*=12.2, 7.8 Hz, 1 H)

2-(4-Fluorophenyl)tetrahydrofuran [Table 3.2, entry 6]

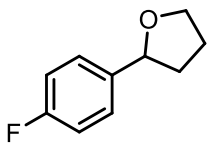

Prepared according to the general procedure, 4-fluorophenylboronic acid (42 mg, 0.3 mmol), K_3PO_4 (64 mg, 0.3 mmol), $NiCl_2$(dtbbpy) (10

mol%), di-tert-butyl peroxide (82 µL, 0.45 mmol) in THF (3 mL) afforded the title compound as a colorless liquid (Concentrated yield = 84%)

^{1}H NMR (chloroform-d, 400 MHz): δ = 7.27 - 7.33 (m, 2 H), 6.98 - 7.04 (m, 2 H), 4.85 (t, *J*=7.2 Hz, 1 H), 4.05 - 4.13 (m, 1 H), 3.88 - 3.96 (m, 1 H), 2.27 - 2.35 (m, 1 H), 1.96 - 2.06 (m, 2 H), 1.76 ppm (dq, *J*=12.2, 7.9 Hz, 1 H)

2-(4-Trifluoromethylphenyl)tetrahydrofuran [Table 3.2, entry 7]

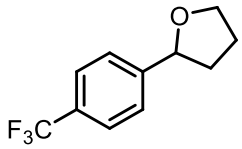

Prepared according to the general procedure, 4-(trifluoromethyl)phenylboronic acid (57 mg, 0.3 mmol), K_3PO_4 (64 mg, 0.3 mmol), $NiCl_2$(dtbbpy) (10 mol%), di-tert-butyl peroxide (82 µL, 0.45 mmol) in THF (3 mL) afforded the title compound as a yellow liquid (Concentrated yield = 51%)

^{1}H NMR (chloroform-d, 400 MHz): δ = 7.53 - 7.60 (m, *J*=8.0 Hz, 2 H), 7.39 - 7.46 (m, *J*=8.0 Hz, 2 H), 4.93 (t, *J*=7.3 Hz, 1 H), 4.05 - 4.13 (m, 1 H), 3.90 - 3.99 (m, 1 H), 2.30 - 2.41 (m, 1 H), 1.95 - 2.06 (m, 2 H), 1.70 - 1.81 ppm (m, 1 H)

2-(2,6-Dimethylmethylphenyl)tetrahydrofuran [Table 3.2, entry 8]

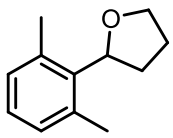

Prepared according to the general procedure, 2,6-dimethylphenylboronic acid (45 mg, 0.3 mmol), K_3PO_4 (64 mg, 0.3 mmol), $NiCl_2$(dtbbpy) (10 mol%), di-tert-butyl peroxide (82 µL, 0.45 mmol) in THF (3 mL) afforded the title compound as a needlelike solid (Concentrated yield = 20%)

^{1}H NMR (chloroform-d, 400 MHz): δ = 7.12 (t, *J*=6.3 Hz, 1 H), 6.91 - 6.99 (m, 2 H), 5.30 (br. s., 1 H), 2.41 - 2.53 (m, 2 H), 2.33 (br. s., 6 H), 2.26 (d, *J*=18.6 Hz, 1 H), 1.22 - 1.29 (m, 1 H), 0.99 - 1.22 ppm (m, 2 H)

3.7.E. General Procedure for the Nickel Catalyzed Cross-Coupling of Phenylboronic Acid and Other C(sp^3)-H Bond Partners

An oven dried 10 mL Schlenk flask was quickly charged with 6.6 mg of $NiCl_2$(glyme) and 8 mg of 4,4'-Di-tert-butyl-2,2'-dipyridyl before dissolution with 3.0 mL of THF via syringe. The solution was then heated to a boil with a heat gun, until the complex completely dissolved and the solution turned dark green. The flask was then placed on a rotary evaporator and allowed to dry under vacuum to produce light green crystals. After evaporation, phenylboronic acid (37 mg, 0.3 mmol) and K_3PO_4 (64 mg, 0.3 mmol) were quickly added to the flask along with a magnetic stir bar before syringing in 3.0 mL of the C(sp^3)-H bond coupling partner and capping with a rubber septum. The solution was then purged under argon for 15 minutes and lastly loaded with di-tert-butyl peroxide (82 µL, 0.45 mmol) via micro syringe. The flask was afterward sonicated until no more solids were visible settling at the bottom of the flask (about one minute). The mixture was irradiated by a solar simulator for 20 hours while stirring at room temperature at an angle of approximately 30^o. The catalyst, base and borates were separated by filtering the crude mixture through a short pad of Celite under reduced pressure into a round bottom flask. The remaining clear liquid was concentrated under reduced pressure on a rotary evaporator.

2-Phenyl-1,4-dioxane [Table 3.3, entry 1]

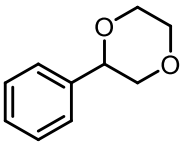

Prepared according to the general procedure, phenylboronic acid (37 mg, 0.3 mmol), K_3PO_4 (64 mg, 0.3 mmol), $NiCl_2$(dtbbpy) (10 mol%), di-tert-butyl peroxide (82 µL, 0.45 mmol) in dioxane (3 mL) afforded the title compound as a colorless liquid (Concentrated yield = 80%)

^{1}H NMR (chloroform-d, 400 MHz): δ = 7.33 - 7.37 (m, 4 H), 7.32 (dd, *J*=8.1, 4.4 Hz, 1 H), 4.62 (dd, *J*=10.2, 2.7 Hz, 1 H), 3.72 - 3.96 (m, 6 H), 3.43 - 3.51 ppm (m, 1 H)

2-Phenyl-1,3-dioxolane [Table 3.3, entry 2]

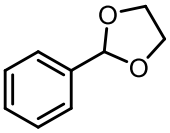

Prepared according to the general procedure, phenylboronic acid (37 mg, 0.3 mmol), K_3PO_4 (64 mg, 0.3 mmol), $NiCl_2$(dtbbpy) (10 mol%), di-tert-butyl peroxide (82 µL, 0.45 mmol) in dioxolane (3 mL) afforded the title compound as a colorless liquid (Concentrated yield = 80%)

^{1}H NMR (chloroform-d, 400 MHz): δ = 7.45 - 7.50 (m, 2 H), 7.35 - 7.38 (m, 4 H), 5.80 (s, 1 H), 4.10 - 4.15 (m, 2 H), 3.99 - 4.06 ppm (m, 2 H)

2-Phenylbenzo[1,3]dioxole [Table 3.3, entry 3]

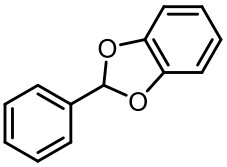

Prepared according to the general procedure, phenylboronic acid (37 mg, 0.3 mmol), K_3PO_4 (64 mg, 0.3 mmol), $NiCl_2$(dtbbpy) (10 mol%), di-tert-butyl peroxide (82 µL, 0.45 mmol) in 1,3-benzodioxole (3 mL) afforded the title compound as a needlelike solid (Concentrated yield = 52%)

^{1}H NMR (chloroform-d, 400 MHz): δ = 7.51 - 7.55 (m, 2 H), 7.34 - 7.39 (m, 3 H), 6.88 (s, 1 H), 6.75 - 6.79 ppm (m, 4 H)

N-benzyl-N-methylaniline [Table 3.3, entry 4]

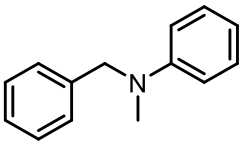

Prepared according to the general procedure, phenylboronic acid (37 mg, 0.3 mmol), K_3PO_4 (64 mg, 0.3 mmol), $NiCl_2$(dtbbpy) (10 mol%), di-tert-butyl peroxide (82 µL, 0.45 mmol) in N,N-dimethylaniline (3 mL) afforded the title compound as a colorless liquid (Concentrated yield = 92%)

^{1}H NMR (chloroform-d, 400 MHz): δ = 7.37 (t, *J*=7.2 Hz, 2 H), 7.28 - 7.34 (m, 1 H), 7.22 - 7.25 (m, 3 H), 7.10 - 7.14 (m, 2 H), 6.61 (br. s., 2 H), 4.42 - 4.49 (m, 2 H), 2.93 ppm (s, 3 H)

N-benzyl-N-methylacetamide [Table 3.3, entry 5]

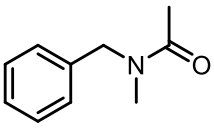

Prepared according to the general procedure, phenylboronic acid (37 mg, 0.3 mmol), K_3PO_4 (64 mg, 0.3 mmol), $NiCl_2$(dtbbpy) (10 mol%), di-tert-butyl peroxide (82 µL, 0.45 mmol) in N,N-dimethylacetamide (3 mL) afforded the title compound as a colorless liquid (Concentrated yield = 57%)

^{1}H NMR (chloroform-d, 400 MHz): δ = 7.25 (br. s., 5 H), 4.53 (br. s., 2 H), 2.85 - 3.01 (m, 3 H), 2.03 ppm (br. s., 3 H)

3.7.F. General Procedure for the Photochemical Synthesis of Nickel Nanoparticles Supported on TiO_2

Nickel nanoparticles supported on TiO_2 were synthesized using a previously described method. P25 TiO_2 (50 mg), benzophenone (22 mg, 0.12 mmol) and $Ni(acac)_2$ (31 mg, 0.12 mmol) were added to a 100 mL Erlenmeyer flask with a magnetic stir bar and diluted with 100 mL of ethanol. The mixture was sonicated for 10 minutes to dissolve the nickel species and benzophenone as well as disperse the TiO_2 into a suspension. The flask was then capped with a rubber septum and purged with argon for 20 minutes. The mixture was placed inside a Luzchem Inc. photoreactor fitted with 14 UVA bulbs and irradiated for 6 hours with stirring. The solution color gradually progressed from pale green to grey. After irradiation, the mixture was transferred to a centrifuge tube and centrifuged at 3500 RPM for 20 minutes to collect the solids. The supernatant was carefully removed, and the solid residue washed with 20 mL of ethanol, followed by redispersion by sonication and further centrifugation. This washing cycle was repeated for a total of 5 times, removing the supernatant with each wash. The resulting solid material was lastly placed in a vacuum desiccator for 72 hours to completely dry the product, affording an approximate 4 wt% loading of nickel nanoparticles.

3.7.G. NMR Data

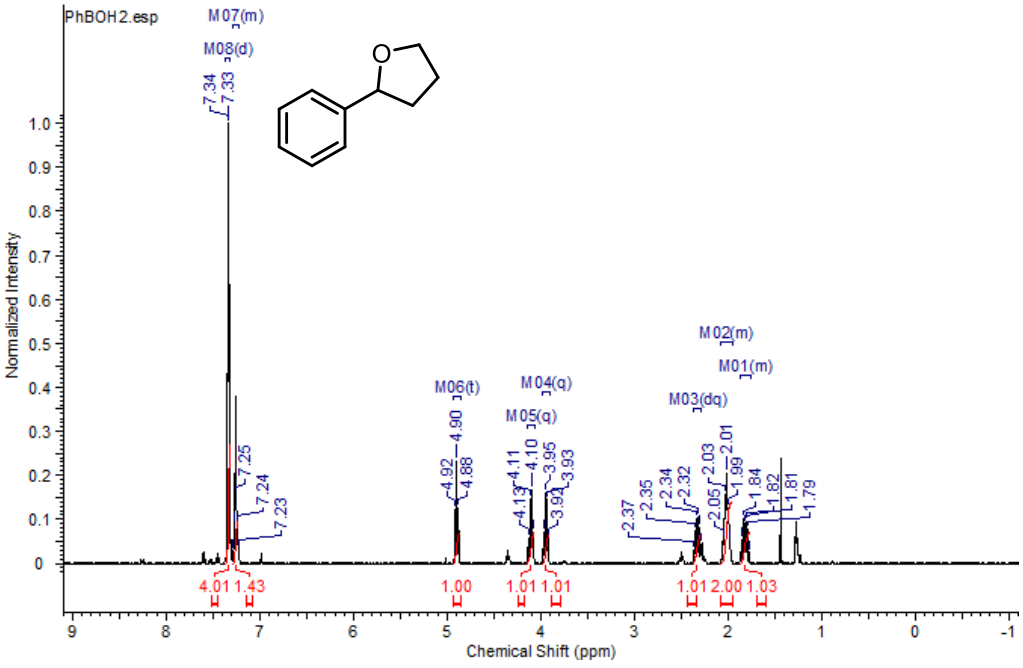

Figure 3A.3. ^{1}H NMR of **product 1** in $CDCl_3$

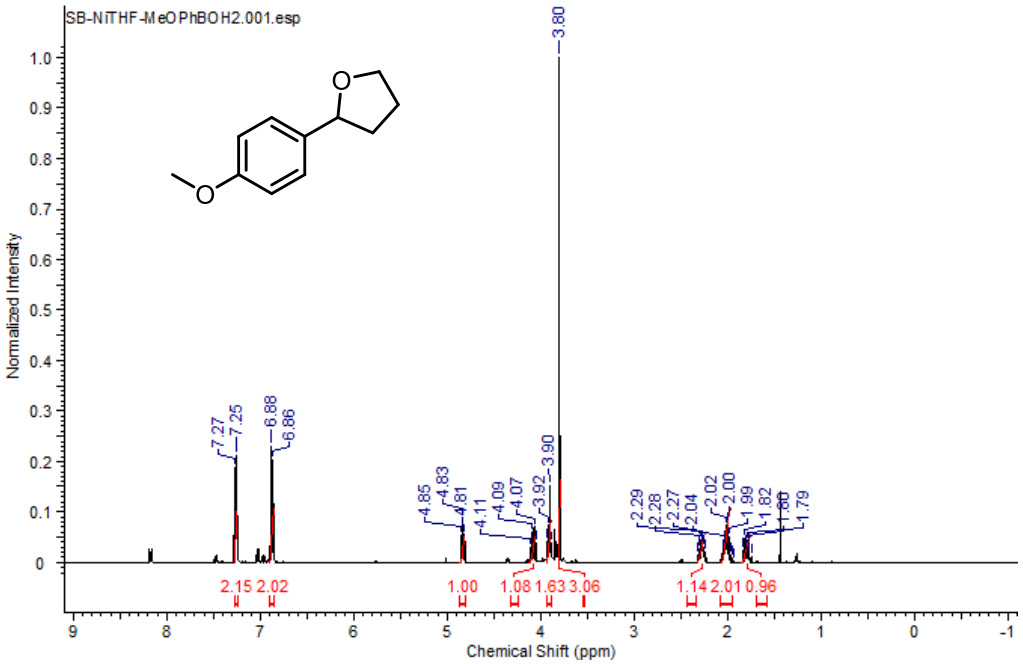

Figure 3A.4. ^{1}H NMR of **product 2** in $CDCl_3$

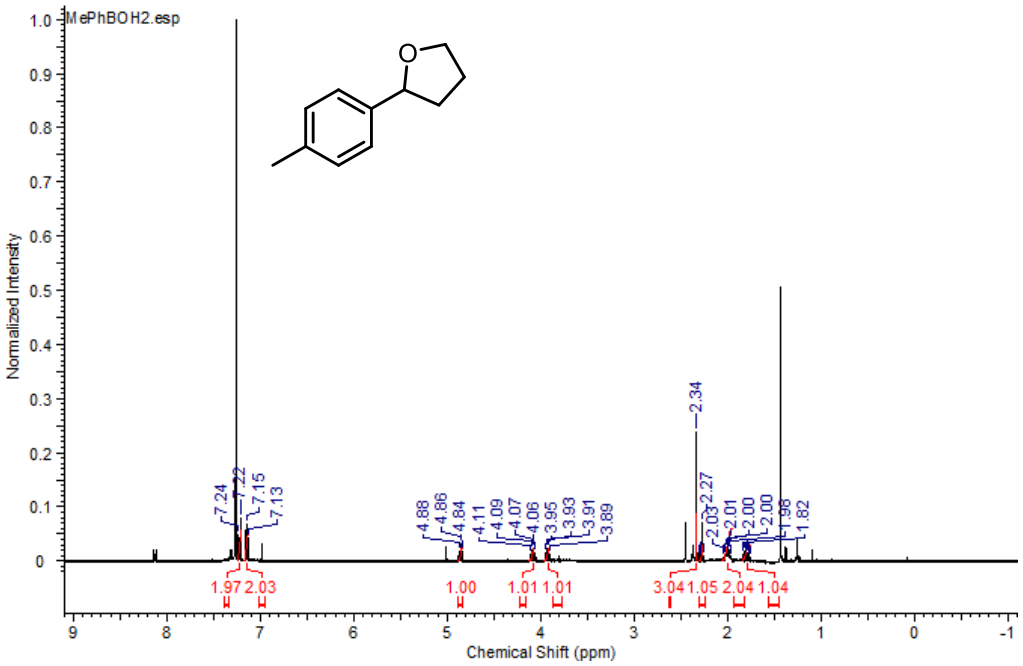

Figure 3A.5. ^{1}H NMR of **product 3** in $CDCl_3$

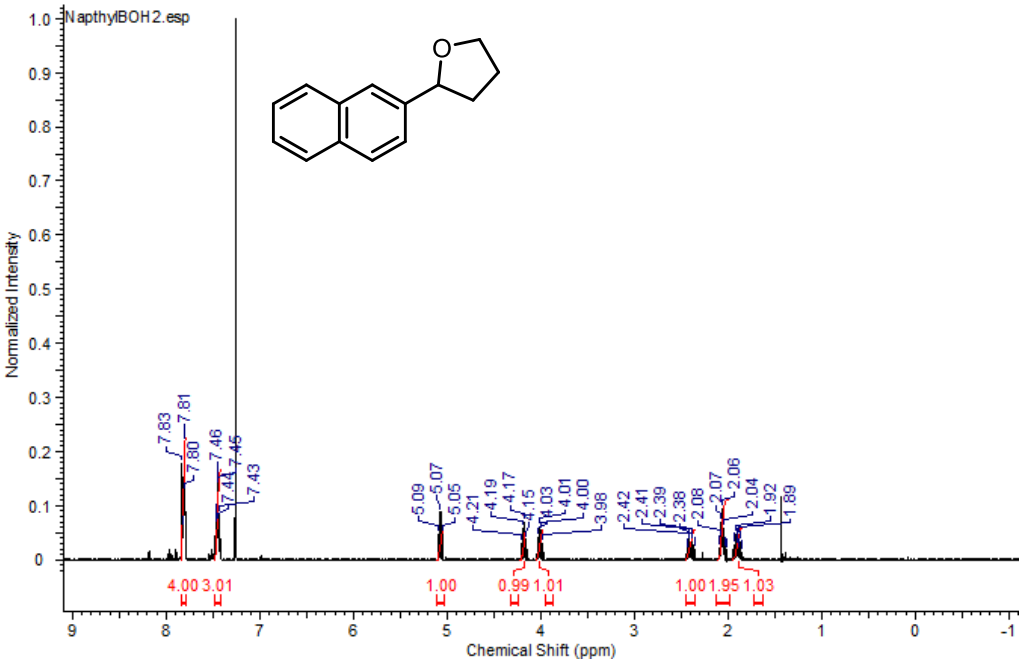

Figure 3A.6. ^{1}H NMR of **product 4** in $CDCl_3$

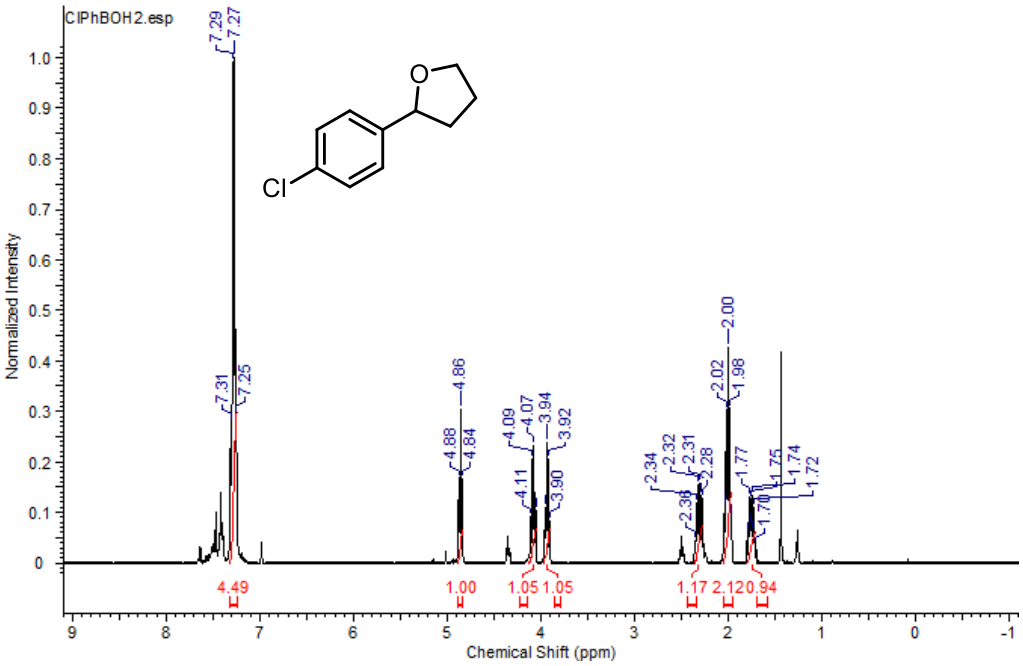

Figure 3A.7. ^{1}H NMR of **product 5** in $CDCl_3$

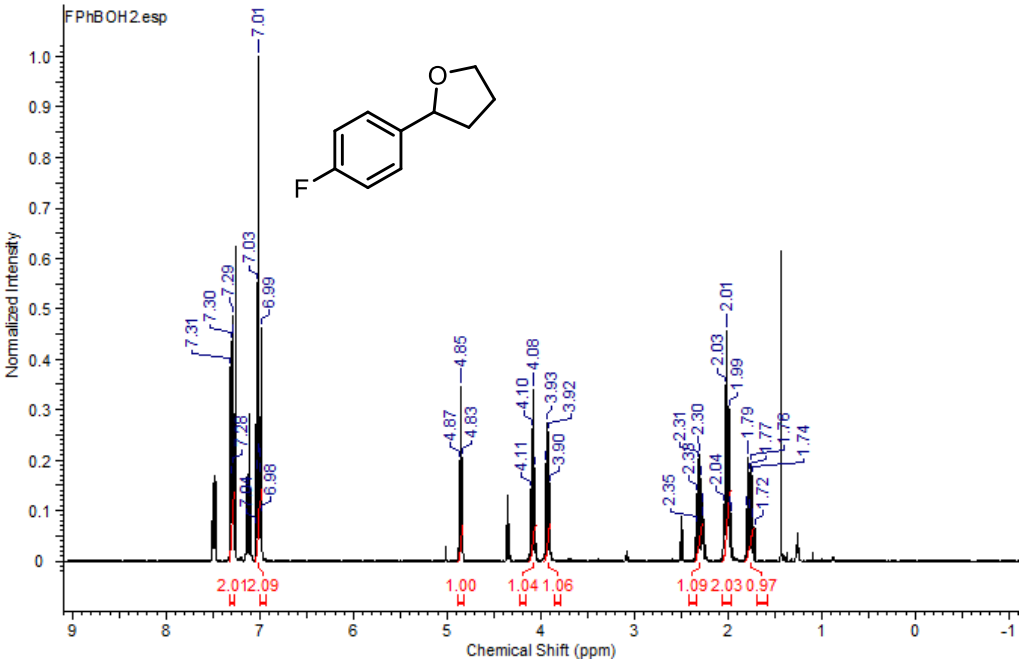

Figure 3A.8. ^{1}H NMR of **product 6** in $CDCl_3$

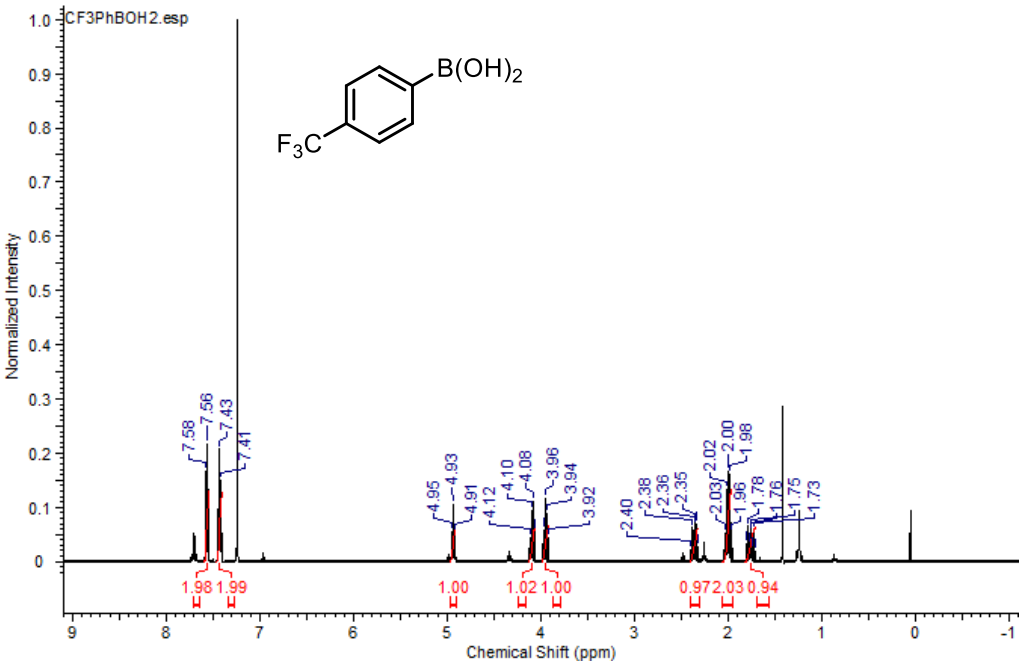

Figure 3A.9. ^{1}H NMR of **product 7** in $CDCl_3$

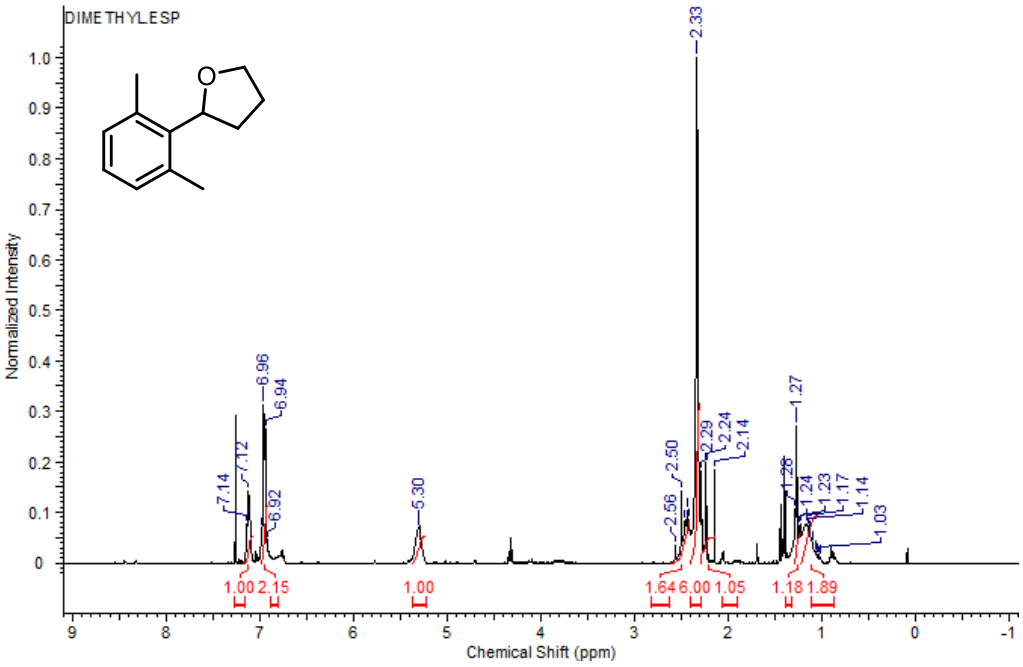

Figure 3A.10. ^{1}H NMR of **product 8** in $CDCl_3$

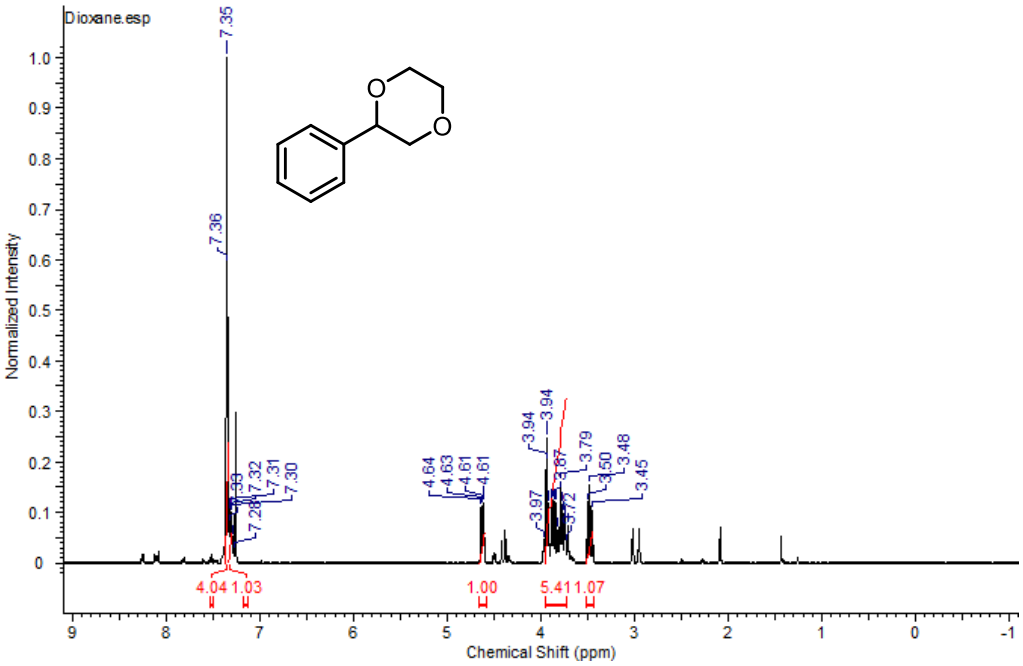

Figure 3A.11. ^{1}H NMR of **product 9** in $CDCl_3$

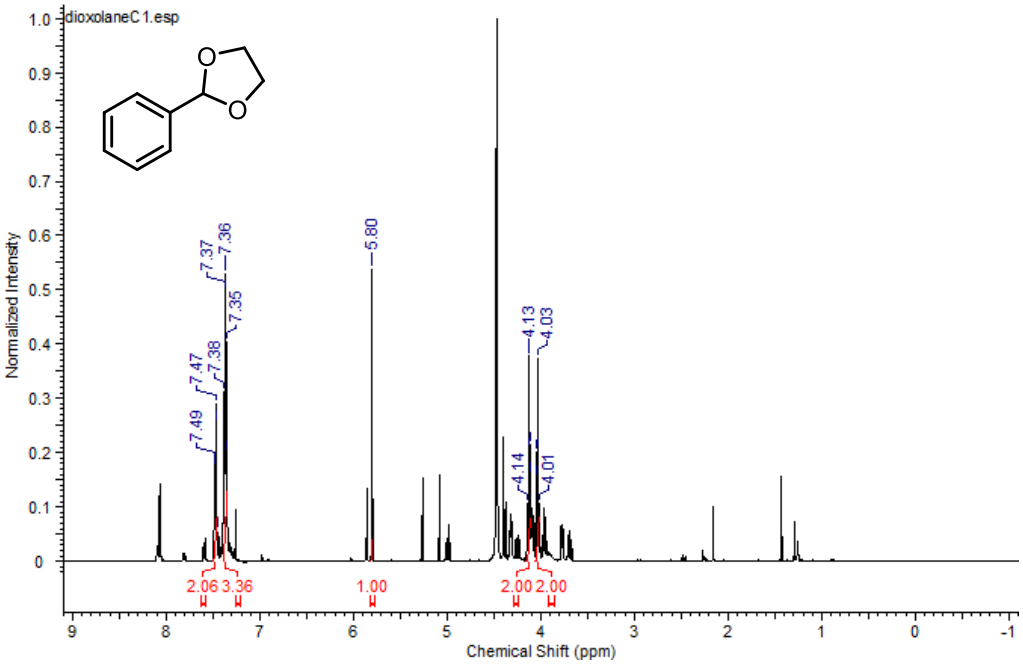

Figure 3A.12. ^{1}H NMR of **product 10** in $CDCl_3$

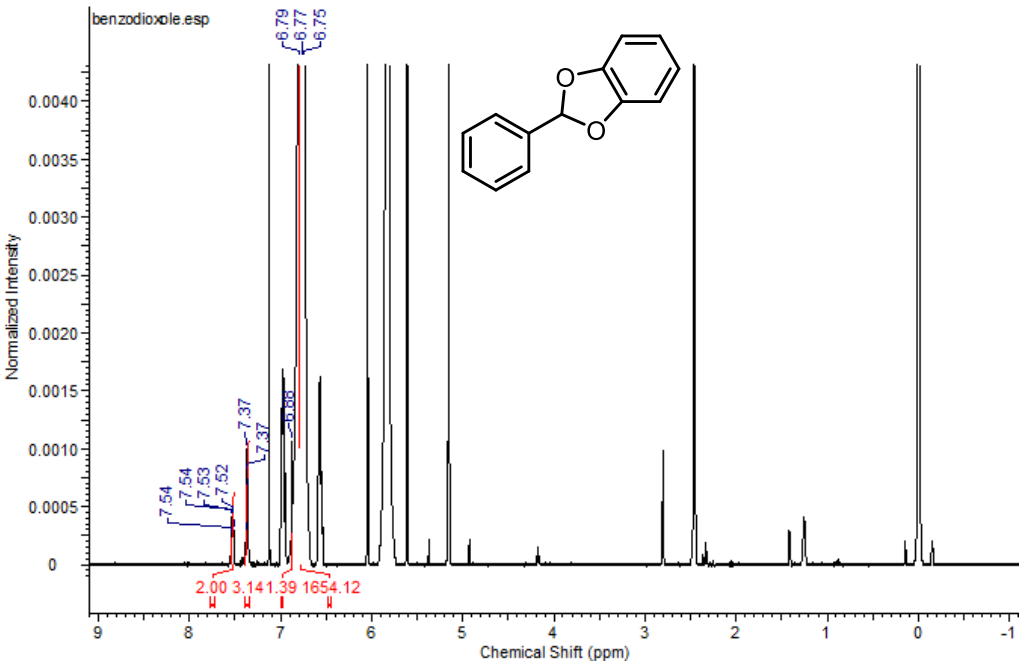

Figure 3A.13. ^{1}H NMR of **product 11** in $CDCl_3$

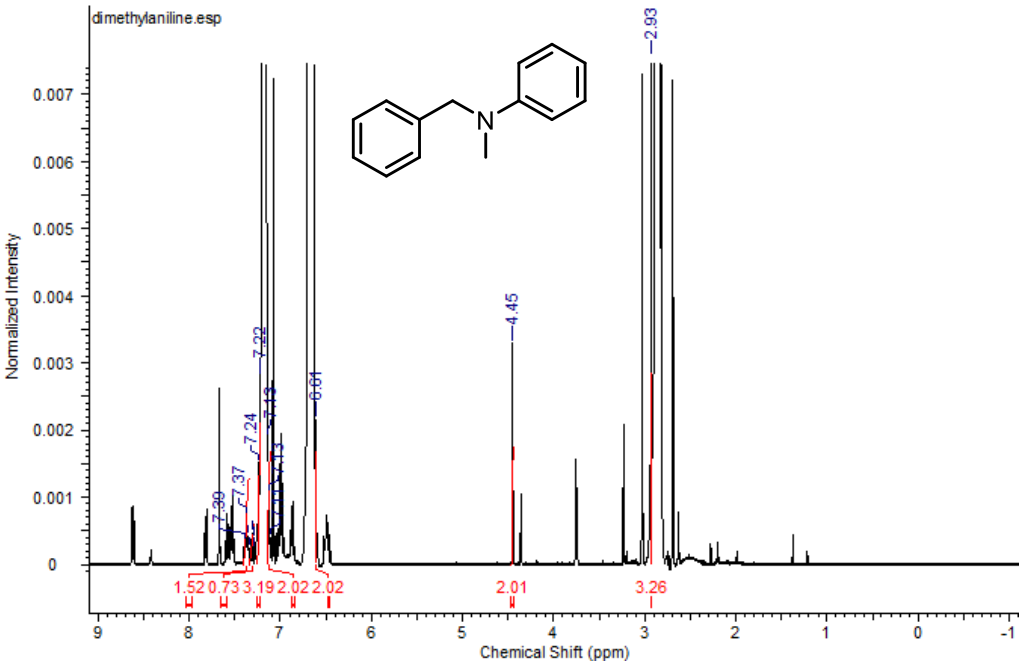

Figure 3A.14. ^{1}H NMR of **product 12** in $CDCl_3$

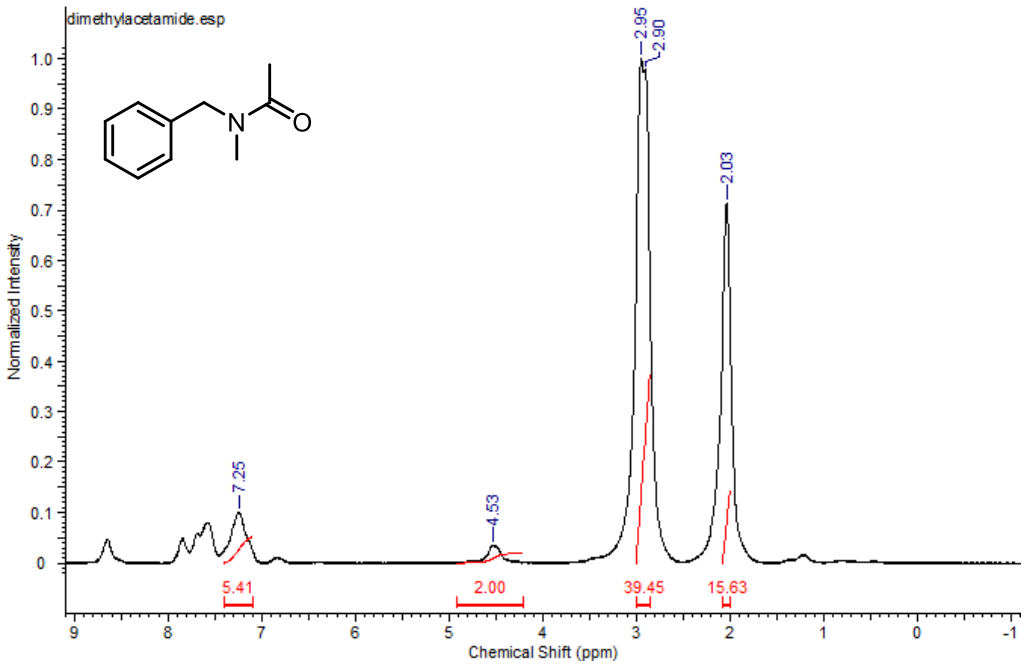

Figure 3A.15. ^{1}H NMR of **product 13** in $CDCl_3$

3.8. References

(1) Heck, K. F.; Nolley, J. P. *J. Org. Chem.* **1972**, *37* (14), 2320–2322.

(2) Sonogashira, K.; Tohda, Y.; Hagihara, N. *Tetrahedron Lett.* **1975**, *16* (50), 4467–4470.

(3) Negishi, E. ichi; King, A. O.; Okukado, N. *J. Org. Chem.* **1977**, *42* (10), 1821–1823.

(4) Milstein, D.; Stille, J. K. *J. Am. Chem. Soc.* **1978**, *100* (11), 3636–3638.

(5) Miyaura, N.; Yamada, K.; Suzuki, A. *Tetrahedron Lett.* **1979**, *20* (36), 3437–3440.

(6) Miyaura, N.; Suzuki, A. *J. Chem. Soc. Chem. Commun.* **1979**, *0* (19), 866–867.

(7) Tellis, J. C.; Primer, D. N.; Molander, G. A. *Science* **2014**, *345* (6195), 433–436.

(8) Noble, A.; McCarver, S. J.; Macmillan, D. W. C. *J. Am. Chem. Soc.* **2015**, *137* (2), 624–627.

(9) Doyle, A. G.; Terrett, J. A.; Zuo, Z.; Chu, L.; MacMillan, D. W. C.; Ahneman, D. T. *Science* **2014**, *345* (6195), 437–440.

(10) Scaiano, J. C.; Wubbels, G. G. *J. Am. Chem. Soc.* **1981**, *103* (3), 640–645.

(11) Liu, L.; Zhang, S.; Chen, H.; Lv, Y.; Zhu, J.; Zhao, Y. *Chem. - An Asian J.* **2013**, *8* (11), 2592–2595.

(12) Gutierrez, O.; Tellis, J. C.; Primer, D. N.; Molander, G. A.; Kozlowski, M. C. *J. Am. Chem. Soc.* **2015**, *137* (15), 4896–4899.

(13) Zuo, Z.; Cong, H.; Li, W.; Choi, J.; Fu, G. C.; MacMillan, D. W. C. *J. Am. Chem. Soc.* **2016**, *138* (6), 1832–1835.

(14) Zacuto, M. J.; Liu, J.; Nielsen, M. K.; Doyle, A. G.; Williams, M. J.; Shields, B. J. *Angew. Chemie Int. Ed.* **2017**, *56* (25), 7191–7194.

(15) Deng, H. P.; Fan, X. Z.; Chen, Z. H.; Xu, Q. H.; Wu, J. *J. Am. Chem. Soc.* **2017**, *139* (38), 13579–13584.

(16) Shields, B. J.; Doyle, A. G. *J. Am. Chem. Soc.* **2016**, *138* (39), 12719–12722.

4. Heterogeneous, Visible Light-Mediated Heck Reactions

4.1. Background

Alkenes, also known as olefins, are important building blocks in synthetic chemistry and among the most produced of all organic chemicals. Many alkenes can be directly synthesized on massive scale from both renewable and fossil-based sources, making them widely accessible and economical feedstock choices.[1] The diverse reactivity of the functional group additionally makes alkenes a valuable reagent with a large number of reactive pathways available to them, usually with high yields and good control of partner selectivity. The alkene bond itself is however quite stable, making the material easy to handle or store. For these qualities, alkenes find themselves frequently used in fine chemicals and pharmaceuticals, as intermediates and final products alike. It is therefore advantageous to directly couple an alkene to another substrate to build larger scaffolds or more complex molecules while leaving the functionality intact.

The use of catalytic alkene C-H bond activation to achieve this goal offers a methodology that is direct and atom-economical whilst mitigating the need for an activating group on the alkene. In particular, the Mizoroki-Heck reaction was developed for the cross-coupling of a terminal olefin with an aryl or alkenyl halide in the presence of a Pd(0) catalyst.[2] The reaction is very effective at preventing migration of the double bond and doubles as one of the few methods capable of synthesizing fused ring systems containing quaternary stereogenic carbon; the Heck reaction remains widely used in the pharmaceutical industry for the generation of large polycyclic structures.[3–5]

The Heck reaction is still not without its limitation - its application has been largely dependent on the use of palladium for a catalyst, which cannot be recovered after use. Another major disadvantage of the system is in the use of phosphine ligands attached to the palladium catalyst that can be both toxic and expensive to the consumer. This catalyst must then be run at elevated temperatures for extended periods, reactions frequently reaching in excess of 130 °C for 24-48-hour reaction times.[6–13] Success has been made in replacing palladium centered catalysts with cheaper base metals like copper or nickel but they are still subject to these unfavorable conditions and may even require specialized additives like ionic liquids or sophisticated activating groups on substrates.[14–16] A previous example of such chemistry proposed that a copper catalyst in high enough loading could thermally produce benzyl radicals from expensive trifluoroborate salts to mediate the coupling to an olefin.[17] This SET based reaction creates a good opportunity for the adaptation of photoredox, and to the best of our knowledge, no previous examples exist of a heterogeneous photocatalytic system for Heck reactions.

With this in mind, we endeavoured to create a catalytic system using gold nanoparticles supported on TiO_2 (Au@TiO_2) that are capable of absorbing visible light, to perform redox transformations. The use of visible light to power these reactions would cut out the requirement for high temperatures needed for catalyst activation. The heterogeneous nature of the catalyst additionally serves to ease the workup process through easy catalyst separation whilst providing recycling capabilities.

4.2. Optimizations and Controls

Titanium dioxide supported gold nanoparticles have previously been demonstrated to catalyze the dimerization of 4-nitrobenzyl bromide using a "quad" green LED array as a light source and N,N-Diisopropylethylamine (DIPEA) as a sacrificial electron donor.[18] We began our study with an attempt to duplicate these results to get a baseline for the reaction conditions necessary for the cross-coupling with an alkene, albeit with an alternative but similar Green light source that contained an array of 7 focused LEDs (LEDi). Initially, only 14% (table 4.1, entry 2) of the dimer could be quantified versus the 81% target to match.

Table 4.1. Effect of Irradiation Time on the Dimerization of 4-Nitrobenzyl Bromide[a]

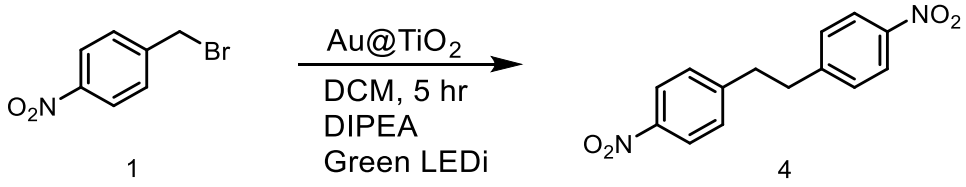

Entry	Time	Yield of Dimer	Conversion
1	1 hr	4%	11%
2	5 hrs	14%	46%
3	20 hrs	5%	100%

[a]Reaction conditions: 4-nitrobenzyl bromide (0.09 mmol), Au@TiO_2 (5 mg), DIPEA (0.18 mmol, 2 eq.), dichloromethane (3 mL). Irradiated with 7 green LED irradiator centered at 525 nm.

This poor result is most likely the outcome of poor power matching from the original light source, which featured 4 high intensity LEDs positioned 90° from each other and focused on a central point. The reaction was repeated at one and twenty hours of irradiation time to probe the reaction's activity with time. Both yield and

conversion of the starting material were reasonably lowered with decreased reaction time but interestingly, the yield also suffered to nearly the same value when allowed to run at four times the standard reaction time. The complete conversion of the starting material at this increased time suggests instability of the product, the dimer alkyl linker potentially being an active cleavage site from radical attack from the still active catalyst. Five hours was chosen as an initial time scale for further optimizations since it allowed for decent conversion of starting material (46%), while avoiding excessive decomposition of the product to probe other changes to the system.

The addition of diphenylethylene was also tested under these baseline conditions to see how our model coupling partner, doubling as a good radical trapping agent, could perform. The reaction was examined with and without the presence of an internal oxidizer that is often necessary in radical oxidative Heck reactions to reform the alkene group in a final step. Only a trace of the cross coupled product was observed when no oxidizer was added to the system (table 4.2, entry 1). The use of di-tert butyl peroxide or manganese dioxide both shut down the production of benzyl dimer and cross coupled product, the former of the two oxidizers also depleting all the diphenylethylene available. In both cases, the oxidizers may work counterproductively by quenching the amine and/or the active catalyst too competitively.

Table 4.2. Table of Oxidizers to Promote Alkene Reformation[a]

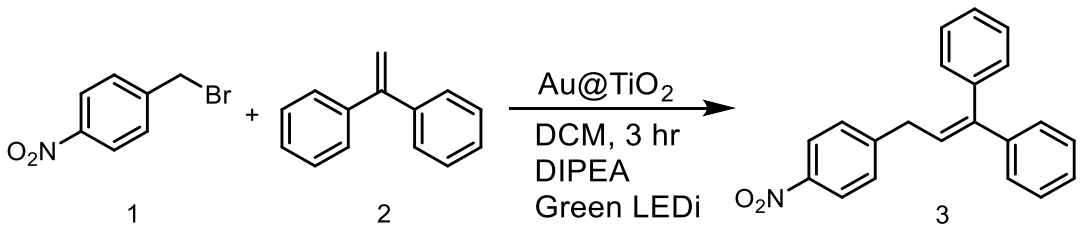

Entry	Oxidant	Yield of Dimer	Conversion	Yield of 3
1	None	10%	40%	trace
2	2 eq. DTBP	trace	37%	ND
3	3 eq. MnO_2	ND	14%	ND

[a]Reaction conditions: 4-nitrobenzyl bromide (0.09 mmol), $Au@TiO_2$ (5 mg), DIPEA (0.18 mmol, 2 eq.), diphenylethylene (0.18 mmol, 2 eq.) dichloromethane (3 mL). Irradiated with 7 green LED irradiator centered at 525 nm. ND: not detected.

Another visible light source was sought out that could prove superior to the incapable green light previously used. A 7 blue LED irradiator was selected as a replacement and would provide approximately four times the irradiance as the green light. First tested at otherwise identical conditions to our baseline for the dimerization (table 4.3, entry 2), an increase in productivity and full conversion of starting material was achieved. The reaction was repeated at three hours to determine if the increased light output might be effective at decomposing the product within a much shorter timescale compared to the green irradiator. Successfully, no product seemed to be decomposing on the short timescale and conversion was only lowered to 89%, a suitable value to continue further optimizations of the system. It should be noted here that 4-nitrobenzylbromide yields 4-nitrotoluene when not converted to either the dimer or heterocoupled product in all examples presented in this chapter.

Table 4.3. Optimization of Reaction Time for Blue Light Irradiation

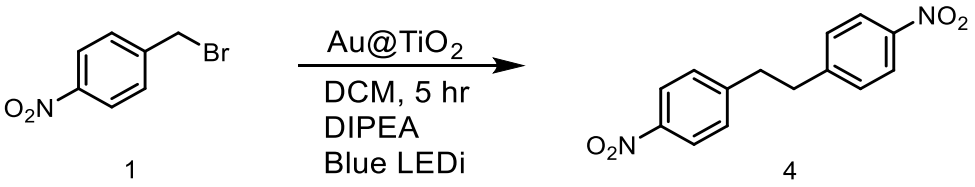

1 4

Entry	Time	Yield of Dimer	Conversion
1	3 hrs	20%	89%
2	5 hrs	20%	100%

Replication of the original dimerization using a green quad LED was not achievable using the prescribed protocol, so a new set of optimizations was performed to adapt to the new conditions and in the presence of an olefin. First, a full screening of light sources was undertaken to identify the most suitable wavelength or intensity available to be used. The 7 blue LED irradiator was found to be the most capable of the light sources selected for screening to perform the dimerization and the cross-coupling, providing 6% yield of the target product (table 4.4, entry 4). In the analysis of the product mixture for entry 4, just as much benzyl dimer was detected relative to running the system without the olefin. The amount of coupled olefin about doubled when a second equivalent of precursor benzyl bromide was added, it was intended that the increased population of benzyl radicals formed would be more likely intercepted by diffusing olefin in solution (entry 5). Additionally, the reduced form of the product, lacking the unsaturation at the coupling site, was detected in an almost equal amount to the target itself.

The use of ultraviolet light on the system consumed all the benzyl bromide starting material but did not result in the formation of either dimer or coupled olefin. In their stead was only a stoichiometric amount of nitrotoluene, its reduced form. Swapping out the 7 blue LED irradiator for a single blue LED was also capable of producing a small amount of the coupled olefin but only in a just detectable amount. The amount of dimer produced also dropped by half, even though the starting material was fully consumed. As a control, the reaction was found to not undergo any changes when allowed to stir in the dark, even after 24 hours.

Table 4.4. Optimization of Light Source[a]

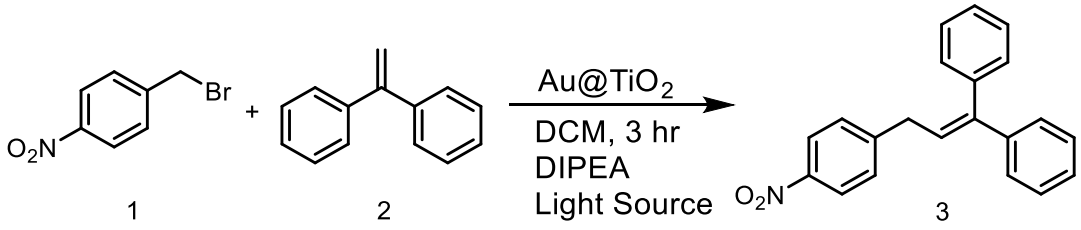

1 2 3

Entry	Light Source	Yield of 3	Yield of Benzyl Dimer	Yield of Reduced Product
1	368 LED	ND	ND	ND
2	Green LEDi	trace	14%	ND
3	465 LED	trace	10%	ND
4	Blue LEDi	6%	20%	trace
5	Blue LEDi	13%	23%	11%[b]
6	Dark	ND	ND	ND[a, c]

[a]Reaction conditions: 4-nitrobenzyl bromide (0.09 mmol), Au@TiO_2 (5 mg), DIPEA (0.18 mmol, 2 eq.), dichloromethane (3 mL). Irradiated with 7 green LED irradiator centered at 525 nm. [b]Run with 0.18 mmol of 4-nitrobenzyl bromide. [c] 24 h reaction time. ND: not detected.

Having found an appropriate light source, concentrations would need to be further adjusted since it plays a vital role in radical reactivity - the starting material was being consumed but not in the preferred manner. The amount of solvent was initially changed to adjust the concentration of all species equally. A small dilution had a negligible effect on the system but an increase in concentration had a slightly more negative outcome in terms of overall productivity.

Table 4.5. Concentration Effects

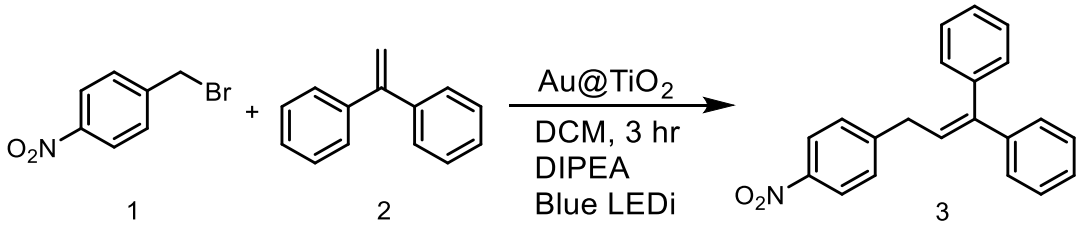

1 2 3

Entry	Eq. of Olefin	Volume	Yield of 3	Yield of Benzyl Dimer
1	0.5	3 mL	13%	23%
2	0.5	2 mL	9%	17%
3	0.5	4 ml	12%	22%

Given that the benzyl radicals required for coupling with the olefin are generated on the surface of the catalyst, it would be inevitable that increasing the concentration of this precursor would quickly give diminishing returns as the radical population density increases near the particle surface only, leading to more dimerization events instead of diffusion of the radical species throughout the medium. It would be advantageous then, to increase the relative amount of olefin in solution to increase the probability of radical interception without increasing dimer events.

Setting the radical precursor as the limiting reagent did offer a small boost to the production of the intended cross-coupling product (Table 4.6, entry 6) and further suppressed the formation of the radical dimer, the formation of the reduced cross coupled product also increased to 17% under these conditions. The formation of either of these products was not greatly affected by the introduction of air when allowed to run under atmosphere, only slightly reducing yields (Table 4.6, entry 5). This result implies that oxygen is poor at oxidizing the proposed coupled radical intermediate to the final product but nonetheless makes the system much more attractive as it shows good tolerance toward atmospheric conditions. Increasing the olefin loading to 10 equivalents further improved yield but not significantly, only reaching 30% productivity and resulting in an unchanged amount of reduced product.

Only about half of the radical precursor was overall detected to undergo some kind of heterocoupling with the olefin and almost no dimerization was observed. The major reactive pathway of the substrate was in forming the dehalogenated decomposition product. In order to help remediate this, we attempted to add the radical precursor stepwise to limit the amount of substrate available at any given time to undergo unproductive events and effectively increase the relative concentration of the olefin. A 45 mM solution of 4-nitrobenzyl bromide in DCM was injected into the reaction mixture setup under the general conditions found in table 4.6 but containing only half the amount of radical precursor. The 4-NBB solution was injected at two 25 mol% doses, first after one hour of irradiation and secondly after two hours of irradiation. The mixture was allowed to stir under illumination for an additional hour to

allow for full consumption of the radical precursor, increasing yield to 40%. When a syringe pump was used to inject a steady amount of substrate over two hours, the yield dropped, suggesting the substrate was beneath a critical concentration.

Table 4.6. General Optimization of Reaction Conditions and Controls[a]

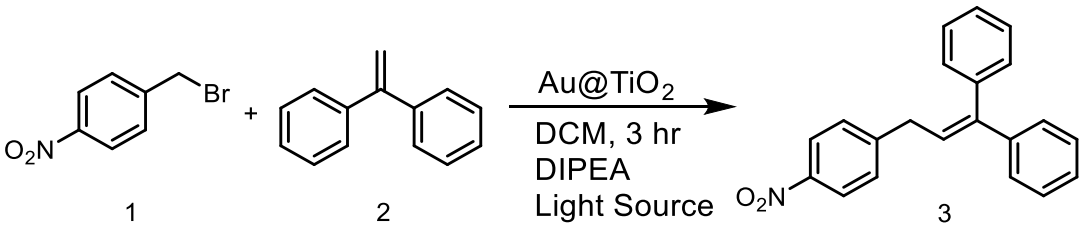

Entry	Eq. of Olefin	Eq. of Amine	Yield of 3	Yield of Benzyl Dimer	Yield of Reduced Product
1	0.5	2.0	13%	11%	trace
2	0.5	1.0	15%	8%	12%
3	0.5	4.0	ND	75%	trace
4	1.0	2.0	6%	10%	trace
5	5.0	2.0	18%	trace	14%[b]
6	5.0	2.0	23%	trace	17%
7	10.0	2.0	30%	trace	17%
8	10.0	2.0	ND	ND	ND[c]
9	10.0	0	10%	trace	ND[d]
10	10.0	0	trace	trace	ND[e]
11	10.0	2.0	40%	trace	17%[f]
12	10.0	2.0	27%	trace	13%[g]

[a]Reaction conditions: 4-nitrobenzyl bromide (0.18 mmol), $Au@TiO_2$ (5 mg), dichloromethane (3 mL). Irradiated with 7 blue LED irradiator centered at 455 nm. [b]Run under atmosphere. [c]No catalyst. [d]No electron donor. [e]3 mL diethyl ether used as solvent and electron donor. [f]25 mol% of 4-nitrobenzyl bromide added after one- and two-hour irradiation time, respectively, to a mixture containing 50 mol% of substrate. [g]4-Nitrobenzyl bromide injected via syringe pump at a rate of 50 mol%/h. ND: not detected.

Performing controls at this stage revealed that omission of the catalyst from the reaction medium completely shut down reactivity. Interestingly, exclusion of the electron donor did not (Table 4.6, entry 9). With the reaction system better optimized, the effect of electron donor loading was examined more closely to observe its effect on the selectivity of the reaction. As seen before, increasing the loading of DIPEA increased the formation of dimer product while suppressing the heterocoupled target (Table 4.7, entry 1). Decreasing the donor loading to one equivalent conversely swapped the selectivity to produce almost no dimer but much more of the cross-product. Further reductions in loading to only half an equivalent diminished yield slightly but resulted in little over 50% conversion of the radical precursor; only a trace of the reduced cross-product could also be detected.

Doubling the irradiation time to 6 hours did improve consumption of 4-Nitrobenzyl bromide but decreased yield of the target significantly. The increase in nitrotoluene production and decomposition of the product under these circumstances could be explained by benzyl radicals competitively abstracting hydrogen from any formed product in a premature radical termination step and foregoing any further propagation. One equivalent of DIPEA was selected as the best loading for the electron donor for these reasons.

Table 4.7. Optimization of Electron Donor Loading[a]

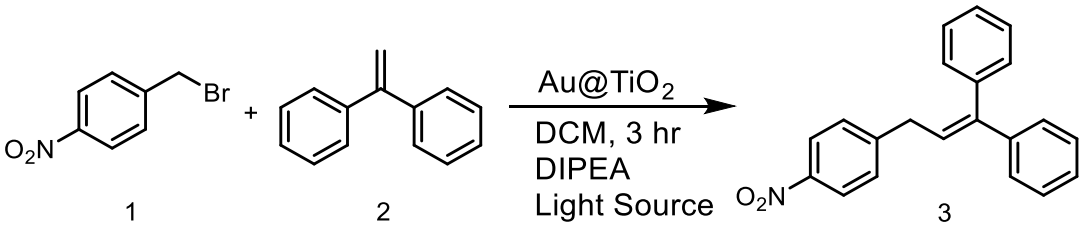

1 2 3

Entry	Eq. of Amine	Yield of 3	Yield of Reduced Product
1	4.0	21%	12%
2	2.0	30%	17%
3	1.0	40%	9%
4	0.5	35%	trace
5	0.5	24%	trace[b]

[a]Reaction conditions: 4-nitrobenzyl bromide (0.18 mmol), diphenylethylene (1.8 mmol), Au@TiO_2 (5 mg), dichloromethane (3 mL). Irradiated with 7 blue LED irradiator centered at 455 nm. [b]Irradiated for 6 hours.

Adjustments to the loading of the radical precursor, olefin, and electron donor thus far had all generated small improvements to forcing a preferred selectivity in the catalytic system toward the desired product. More work was still needed however, to determine a proper concentration for all the necessary reactive materials not only to improve yield but ideally lower the high loading of olefin needed for adequate production. The concentration of 4-nitrobenzyl bromide was increased from 60 mM to 100 mM and immediately showed improvement (Table 4.8, entry 2), although increasing beyond this point to 167 mM did not.

Table 4.8. Optimization of Olefin Loading[a]

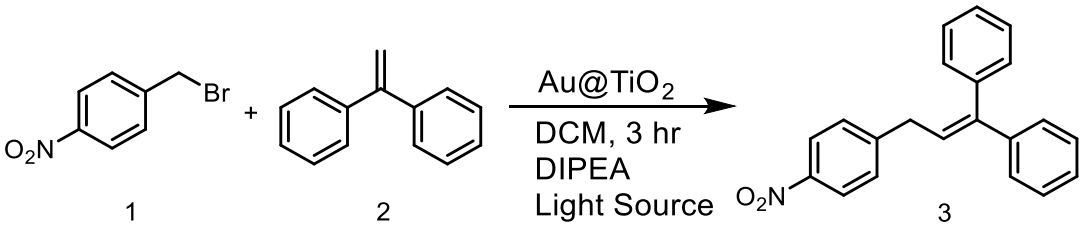

1 2 3

Entry	[Benzyl Bromide]	Eq. of Olefin	Yield of 3	Yield of Reduced Product
1	60 mM	10.0	40%	9%
2	100 mM	10.0	50%	13%
3	167 mM	10.0	50%	10%
4	100 mM	5.0	51%	12%
5	100 mM	2.0	27%	11%

[a]Reaction conditions: 4-nitrobenzyl bromide (0.18 - 0.5 mmol), diphenylethylene (0.6 - 5 mmol), DIPEA (0.18 – 0.5 mmol, 1 eq.), Au@TiO_2 (5 mg), dichloromethane (3 mL). Irradiated with 7 blue LED irradiator centered at 455 nm.

The loading of olefin was twice reduced at 100 mM 4-NBB concentration, at 5 equivalents the outcome was practically unchanged from using 10. Dropping the loading of diphenylethylene to only two equivalents drastically lowered yield and significantly reduced its practicality.

4.3. Scope of Vinyl Arenes

With many optimization steps performed and moderate production of a model cross-coupled olefin achieved, we decided to apply this system to other olefins to see what impact other functionalities might have on reactivity.

Table 4.9. Au@TiO_2 Catalyzed Oxidative Heck Reactions: Scope of Vinylarenes[a]

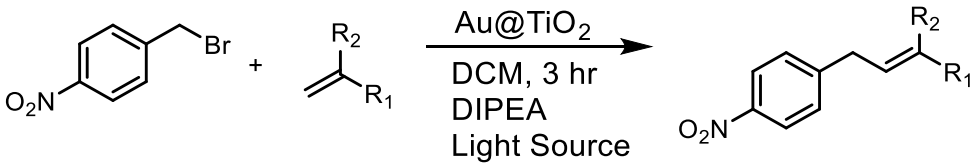

Entry	Olefin	Product	Yield
1		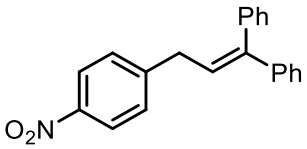	51%
2	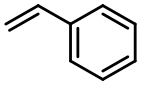	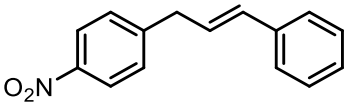	trace
3	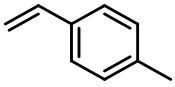	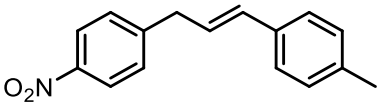	trace
4	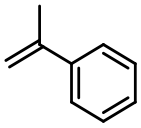	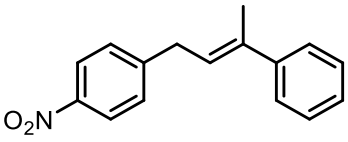	trace
5	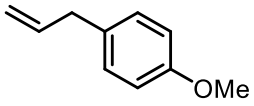	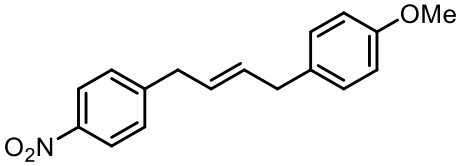	trace
6	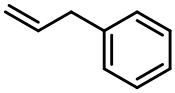	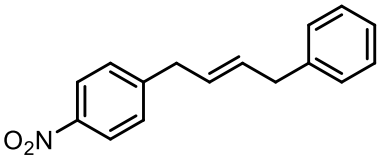	trace

[a]Reaction conditions: 4-nitrobenzyl bromide (0.3 mmol), diphenylethylene (1.5 mmol), DIPEA (0.3 mmol), Au@TiO_2 (5 mg), dichloromethane (3 mL). Irradiated with 7 blue LED irradiator centered at 455 nm for 3 hours.

Unfortunately, all olefins applied to the catalytic system only produced a trace amount of the heterocoupled product. Many of these olefins are capable of undergoing

polymerization with the exception of α-methylstyrene and this characteristic would be a reasonable explanation for low productivity but very little conversion of any of these materials was detected at all. With full conversion of the radical precursor into nitrotoluene, the inactivity can be attributed to poor propagation of the benzyl radical with the olefin in an addition step or poor stability of the resulting intermediate.

4.4. Mechanistic Insights

Scheme 4.1 displays a plausible mechanism for the oxidative Heck reaction catalyzed by Au@TiO_2 whereby the gold nanoparticles absorb visible light to promote the excitation of electrons. These electrons may rapidly migrate to the support, TiO_2, where they are stalled from recombining with the photogenerated hole in the gold nanoparticle, increasing its lifetime. Benzylbromide can engage this electron on the support to form a bromide ion and a benzyl radical while the electron donor replenishes the electronic deficiency in the catalyst. At this stage, the benzyl radical can propagate in a radical addition step with an olefin to form a new alkyl radical intermediate. Oxidation of this molecule is required to remove the radical and regenerate the alkene functionality. After electron donation to the catalyst, DIPEA may accept this electron and perform the oxidative step, turning over the catalytic cycle.

Scheme 4.1. Proposed Mechanism for the Au@TiO_2 Catalyzed Oxidative Heck Reaction

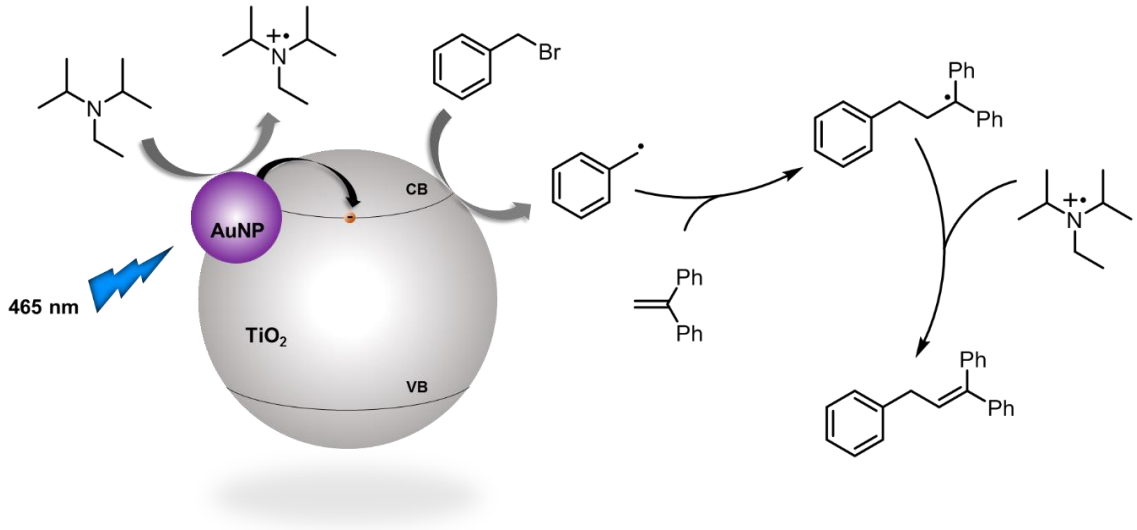

We can rationalize the effect the electron donor loading has on this system by the competitive second oxidation of the α-amino radical that forms after quenching of the catalyst. The α-amino radical is generated by deprotonation of the amine radical cation and is a potent reducing agent capable of reducing 4-nitrobenzyl bromide.[19-22] As depicted in scheme 4.2, this reduction step would generate benzyl radicals, much like the catalyst is intended to do. Implementing more than one equivalent of the electron donor may therefore produce too many benzyl radicals too quickly, consuming the substrate and generating more of the benzyl dimer. Opposingly, too little electron donor may not adequately replenish the electrons in the catalyst, lowering its effectiveness and overall activity.

Scheme 4.2. Competitive Second Oxidation of the α-amino Radical

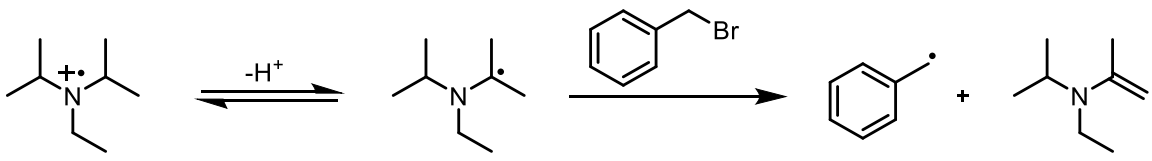

4.5. Conclusion

In this chapter, we have illustrated how the oxidative Heck reaction, dominated by homogeneous catalysts requiring high heat for activation, can be translated into a heterogeneous, photoredox based system using gold nanoparticles supported on titanium dioxide. Although the scope is highly restricted and the yields moderate, this work still provides a proof-of-concept for the adaptation of an important catalytic manifold to using much milder conditions and more ubiquitous materials. Facile catalyst separation, the prospect of catalyst recyclability and short reaction times also make this system more attractive.

4.6. Appendix

4.6.A. General Information

Substrates and Reagents: 4-nitrobenzyl bromide, N,N-Diisopropylethylamine (DIPEA), diphenylethylene and all substrates were purchased from commercial suppliers (Sigma Aldrich, Alfa Aesar, Strem and Fisher) and used as received with no purification. Titanium dioxide supported gold nanoparticles (1%) were purchased as extrudates from Strem and grinded into a fine powder by agate mortar and pestle before use.

Light Sources: Blue light illumination was performed using a Luzchem Inc. LEDi-HBL fitted with a 7 blue LED head operating at 25,400 W/m^2 light power intensity centered at 455 nm. The corresponding 7 green LED head was used for irradiation centered at 525 nm at 6,810 W/m^2.

Automated Injection: Reagent solution was injected using an NE-300 syringe pump by New Era Pump Systems.

Chromatography: Preparatory thin layer chromatography (PTLC) was performed using 1,000 µm thick silica on glass baked TLC plates purchased from Millipore.

NMR: All ^{1}H NMR were recorded on a Bruker Avance 400 spectrometer. Chemical shifts (δ) are reported in ppm from the solvent.

4.6.B. Diffuse Reflectance Spectrum of $Au@TiO_2$

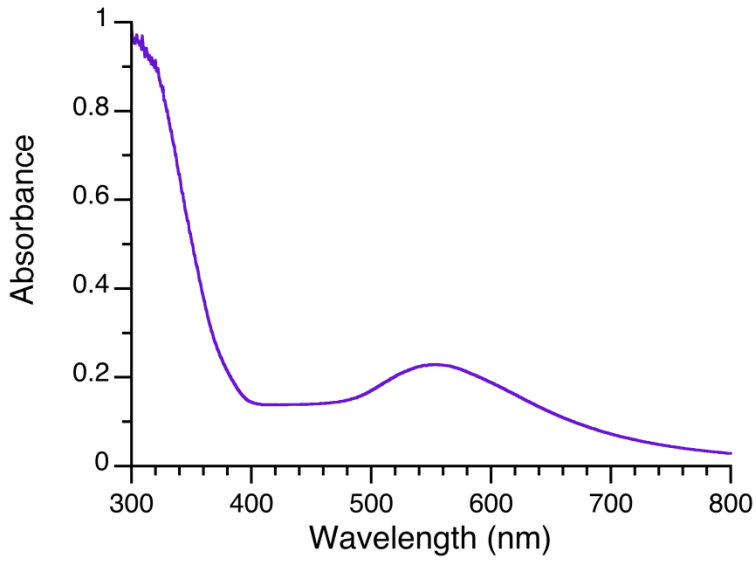

Figure 4A.1. Normalized diffuse reflectance spectrum for commercial titanium dioxide supported gold nanoparticles.

4.6.C. General Procedure for the $Au@TiO_2$ Catalyzed Oxidative Heck Reaction of Benzyl Halides and Vinylarenes

Commercial $Au@TiO_2$ was prepared for use by grinding a few pellets of the extrudates in an agate mortar and pestle for 20 minutes. 4-Nitrobenzyl bromide (65 mg, 0.3 mmol) and 5 mg of grinded $Au@TiO_2$ were then added to a 10 mL test tube. To this, diphenylethylene (265 µL, 1.5 mmol) was added by micro syringe before dilution with 3 mL of dichloromethane and capping with a rubber septum. The sample was purged with argon for 10 minutes, then N,N-Diisopropylethylamine (52 µL, 0.3 mmol) was syringed into the tube before wrapping with parafilm. The container was sonicated for several minutes to disperse the heterogeneous catalyst and placed on a focused 7 blue LED irradiator for 3 hours. A stream of air was allowed to pass over the reaction vessel during irradiation to keep temperatures at 30 °C or lower, no boiling of the solvent was observed. The completed reaction was diluted with DCM and transferred to a 15 mL

centrifuge tube before being spun at 10,000 RPM for 5 minutes to separate the solid catalyst from the rest of the reaction mixture. The supernatant was transferred to a round bottom flask and the solid catalyst washed with additional dichloromethane to extract any remaining organics from the catalyst surface. The washings were combined, and the solvent evaporated under reduced pressure.

<u>1-(4-nitrophenyl)piperidine</u> [Table 4.9, entry 1]

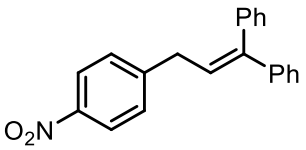

Prepared according to the general procedure, 4-Nitrobenzyl bromide (65 mg, 0.3 mmol), Au@TiO_2 (5 mg), diphenylethylene (265 µL, 1.5 mmol), N,N-Diisopropylethylamine (52 µL, 0.3 mmol) in DCM (3 mL) afforded the title compound as a colorless liquid (Concentrated yield = 51%)

^{1}H NMR (chloroform-d, 400 MHz): δ = 8.13 - 8.17 (m, 2 H), 7.37 - 7.42 (m, 2 H), 7.20 - 7.31 (m, 13 H), 6.22 (t, *J*=7.5 Hz, 1 H), 3.57 ppm (d, *J*=7.6 Hz, 2 H)

4.6.D. NMR Data

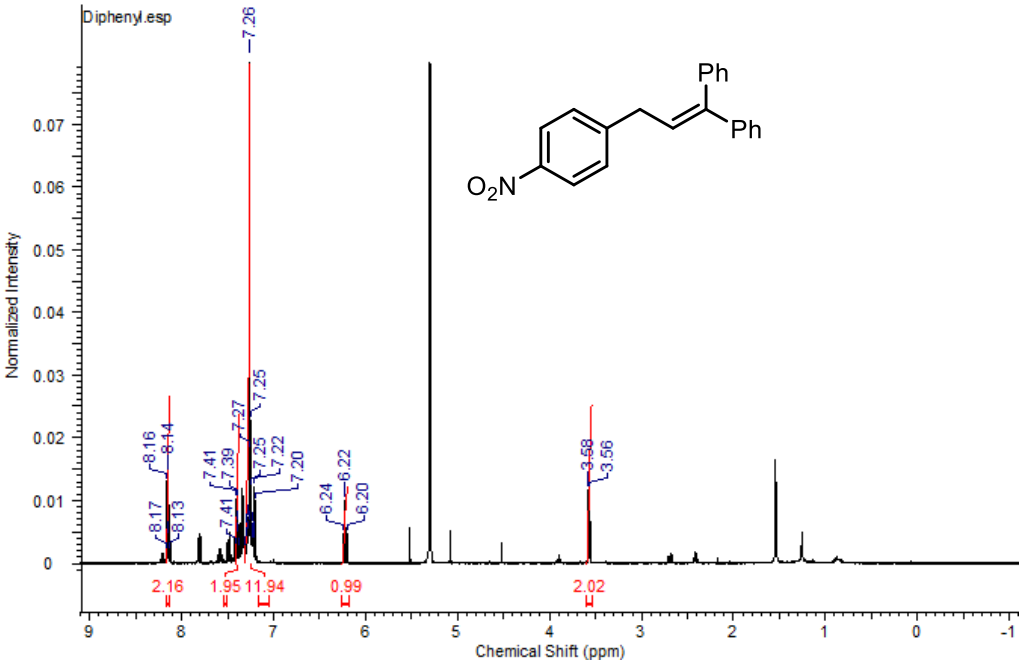

Figure 4A.2. ^{1}H NMR of **product 1** in $CDCl_3$

4.7. References

(1) Wade, L. G. *Organic Chemistry*, 6th ed.; Pearson Prentice Hall: Upper Saddle River, 2006.

(2) Heck, K. F.; Nolley, J. P. *J. Org. Chem.* **1972**, *37* (14), 2320–2322.

(3) Dounay, A. B.; Overman, L. E. *Chem. Rev.* **2003**, *103* (8), 2945–2964.

(4) Torborg, C.; Beller, M. *Adv. Synth. Catal.* **2009**, *351* (18), 3027–3043.

(5) Peterson, E. A.; Overman, L. E. *Proc. Natl. Acad. Sci.* **2004**, *101* (33), 11943–11948.

(6) Fayol, A.; Fang, Y. Q.; Lautens, M. *Org. Lett.* **2006**, *8* (19), 4203–4206.

(7) Liu, S.; Berry, N.; Thomson, N.; Pettman, A.; Hyder, Z.; Mo, J.; Xiao, J. *J. Org. Chem.* **2006**, *71* (19), 7467–7470.

(8) Sabounchei, S. J.; Ahmadi, M.; Azizi, T.; Panahimehr, M. *Synlett* **2014**, *25* (3), 336–342.

(9) Cui, X.; Li, J.; Zhang, Z. P.; Fu, Y.; Liu, L.; Guo, Q. X. *J. Org. Chem.* **2007**, *72* (24), 9342–9345.

(10) Karimi, B.; Enders, D. *Org. Lett.* **2006**, *8* (6), 1237–1240.

(11) Yu, L.; Huang, Y.; Wei, Z.; Ding, Y.; Su, C.; Xu, Q. *J. Org. Chem.* **2015**, *80* (17), 8677–8683.

(12) Wang, A. E.; Xie, J. H.; Wang, L. X.; Zhou, Q. L. *Tetrahedron* **2005**, *61* (1), 259–266.

(13) Battace, A.; Zair, T.; Doucet, H.; Santelli, M. *Synthesis (Stuttg).* **2006**, *2006* (20), 3495–3505.

(14) Gu, S.; Ni, P.; Chen, W. *Chinese J. Catal.* **2010**, *31* (8), 875–886.

(15) Inamoto, K.; Kuroda, J.; Hiroya, K.; Noda, Y.; Watanabe, M.; Sakamoto, T. *Organometallics* **2006**, *25* (12), 3095–3098.

(16) Bhanage, B. M.; Zhao, F.; Shirai, M.; Arai, M. *Catal. Letters* **1998**, *54* (4), 195–198.

(17) Liwosz, T. W.; Chemler, S. R. *Org. Lett.* **2013**, *15* (12), 3034–3037.

(18) Kern, J. M.; Sauvage, J. P. *J. Chem. Soc. Chem. Commun.* **1987**, No. 8, 546–548.

(19) Lanterna, A. E.; Elhage, A; Scaiano, J. C. *Catal. Sci. Technol.,* **2015**, 5, 4336-4340.

(20) Miyake, Y.; Nakajima, K.; Nishibayashi, Y. *J. Am. Chem. Soc.* **2012**, *134* (7), 3338–3341.

(21) Scaiano, J. C. *J. Phys. Chem.* **1981**, *85* (19), 2851–2855.

(22) Ismaili, H.; Pitre, S. P.; Scaiano, J. C. *Catal. Sci. Technol.* **2013**, *3* (4), 935–937.

5. Summary and Future Directions

5.1. Summary

This thesis has investigated three main concepts that can be applied to and greatly benefit the field of organic chemistry, which are summarized in the following passages. The first goal was to implement cheaper catalytic materials to carry out organic transformations. As previously discussed, many catalytic reactions including those based on thermal and photo activation require expensive noble metals to carry out the synthesis. In chapter 2, we surveyed the use of unmodified alumina to catalyze nucleophilic aromatic substitution reactions between aryl chlorides and amines. Aryl chlorides are generally the cheapest and most abundant aryl halides available but are usually unfavored due to their low reactivity. Amines are also common but very important building blocks in many chemical products as they are a source of nitrogen and have widespread application. The coalescence of these useful and low-cost feedstocks into a coupling system catalyzed by an earth abundant material provides a widely accessible and economical chemical production stream for useful products. As a bonus, this particular system shows that cobalt is not in fact required to be added to the catalyst for functionality and post modification of alumina is redundant.

In chapter 3, we demonstrated that nickel could be used to carry out reactions previously typical of palladium and other noble metals. Our method, utilizing nickel as an all in one catalyst could indirectly catalyze the activation of C-H bonds and subsequently couple the open carbon sites to various boronic acids. Where one might

expect dual catalysis between two separate catalytic species to play a role, we have succeeded in excluding the need for a separate photosensitizer, streamlining the catalytic process and reducing waste. This system additionally can be powered off solar light, reactions presented in this work were carried out in a solar simulator for reproducibility purposes but were nonetheless able to be catalyzed quite effectively when placed on a window sill during the day.

While gold is not actually a base metal, it is more available and cheaper than many of the other common noble metals used in catalysis. Its implementation in very small loadings in conjunction with very cheap titanium dioxide in chapter 4 showcases another example of a lower cost replacement to an area of chemistry dominated by palladium. There are limited examples of cheap catalysts utilized in the oxidative Heck reaction and where they are available, it is not uncommon to find costly compromises made for their success.

Secondly, the work in this thesis strived to find catalytic systems that facilitate easier workup through superior catalyst separation capabilities. Alumina in any solvent was found to be easily and completely separated from reaction mixtures by suction filtration in chapter 2. When non polar solvents were used, the base could also be just as easily separated from the reaction mixture. Similarly, Au@TiO_2 was easily recovered from crude reaction mixtures by centrifugation, it is also one of the only examples of a heterogeneous catalyst being used in Heck reactions. Unfortunately, in chapter 3, nickel was not successfully heterogenized as a catalyst, nor was palladium when supported on

titanium dioxide. Titanium dioxide was also incapable of carrying out the chemistry on its own by directly engaging with DTBP as was originally intended.

Lastly, and perhaps most importantly, this thesis aimed to develop photoredox based catalytic systems to apply mild reaction conditions. A useful characteristic of many photosensitizers is their ability to be effectively inert without photoexcitation but promote selective and useful activation of other molecules when illuminated. This provides distinct control over reactions with the flick of a switch and increased safety in material handling. At room and mildly elevated temperatures, nickel was not an effective cross-coupling catalyst and required visible light for its operation. For the oxidative Heck reactions studied in chapter 4, Au@TiO_2 was a critical ingredient for any chemistry to happen when visible wavelengths were used. Without illumination, reaction mixtures containing the catalyst did not undergo any significant changes, unperturbed by its presence. The use of this catalyst also completely removed the need for the addition of thermal energy into the reaction system, operating just above room temperature. This provides the added benefit of preventing polymerization from sensitive olefins known to undergo polymerization at elevated temperatures.

5.2. Future Directions

The work presented in this thesis demonstrates that heterogenization, low cost materials and photoredox can be applied to important organic transformations. Despite the advantages these bring, there are still some limitations in the work shown here. Alumina was tested largely as a proof of concept and, despite published reports, did not

require cobalt modification to act as a catalyst. Although successful in this endeavor, a full scope was never carried out to determine its usefulness with other substrates containing diverse functionalities.

In chapter 3, nickel was shown to be a photoactive catalyst but for all its merits, an exhaustive mechanistic analysis of its function was not carried out. A better understanding of the underlying chemistry at work would no doubt foster improvement on this system. Reaction times of 20 hours are relatively short given the reaction conditions but are still long in a broader sense. Optimization of light sources to only those necessary for activation could ameliorate this to some degree and cut down on wasted energy for underutilized wavelengths when using artificial light sources.

The Au@TiO_2 catalyzed Heck reaction demonstrated many of the attractive qualities a heterogeneous photocatalyst can offer. The scope of applicability however, was abysmal, likely due to poor radical intermediate stability when other substrates are used. This catalytic system could benefit from further optimizations, particularly in the suppression of nitrotoluene formation. Mechanistically speaking, much of the proposed chemistry is known but overall becomes convoluted when olefins are added into the mix. A deeper understanding of this area of chemistry specifically would be beneficial for understanding the fundamental flaws in the system and how to address them properly.

5.3. Claims to Original Research

- Development of a catalytic system employing unmodified alumina as catalyst for the coupling of activated aryl chlorides to amines.
- Development of a photocatalytic system employing a nickel complex as a photoactivated cross-coupling catalyst for the activation of C-H bonds and subsequent coupling to boronic acids.
- The first example of heterogeneous photoredox catalysis for the oxidative Heck reaction between 4-nitrobenzyl bromide and diphenylethylene.